Dartmouth College
Dartmouth Digital Commons

Dartmouth Scholarship | Faculty Work

11-20-2012

A Novel Method for Comparative Analysis of Retinal Specialization Traits from Topographic Maps

Bret A. Moore
Purdue University

Jason M. Kamilar
Midwestern niversity

Shaun P. Collin
University of Western Australia

Olaf R. P. Bininda-Emonds
Fakultät V. Carl von Ossietzky University

Nathaniel J. Dominy
Dartmouth College

See next page for additional authors

Follow this and additional works at: https://digitalcommons.dartmouth.edu/facoa

 Part of the Physiology Commons

Dartmouth Digital Commons Citation

Moore, Bret A.; Kamilar, Jason M.; Collin, Shaun P.; Bininda-Emonds, Olaf R. P.; Dominy, Nathaniel J.; Hall, Margaret I.; Hessy, Christopher P.; Johnsen, Sonke; Lisney, Thomas J.; Loew, Ellis R.; and Moritz, Gillian, "A Novel Method for Comparative Analysis of Retinal Specialization Traits from Topographic Maps" (2012). *Dartmouth Scholarship*. 3896.
https://digitalcommons.dartmouth.edu/facoa/3896

This Article is brought to you for free and open access by the Faculty Work at Dartmouth Digital Commons. It has been accepted for inclusion in Dartmouth Scholarship by an authorized administrator of Dartmouth Digital Commons. For more information, please contact dartmouthdigitalcommons@groups.dartmouth.edu.

Authors

Bret A. Moore, Jason M. Kamilar, Shaun P. Collin, Olaf R. P. Bininda-Emonds, Nathaniel J. Dominy, Margaret I. Hall, Christopher P. Hessy, Sonke Johnsen, Thomas J. Lisney, Ellis R. Loew, and Gillian Moritz

This article is available at Dartmouth Digital Commons: https://digitalcommons.dartmouth.edu/facoa/3896

A novel method for comparative analysis of retinal specialization traits from topographic maps

Bret A. Moore Dept. of Biological Sciences, Purdue Univ., West Lafayette, IN, USA

Jason M. Kamilar Dept. of Anatomy, Midwestern Univ., Glendale, AZ, USA; School of Human Evolution & Social Change, Arizona State Univ., Tempe, AZ, USA

Shaun P. Collin School of Animal Biology & UWA Oceans Institute, The Univ. of Western Australia, Crawley, WA, Australia

Olaf R. P. Bininda-Emonds AG Systematik & Evolutionsbiologie, IBU - Fakultät V. Carl von Ossietzky Univ., Oldenburg, Germany

Nathaniel J. Dominy Dept. of Anthropology, Dartmouth College, Hanover, NH, USA

Margaret I. Hall Dept. of Physiology, Midwestern Univ., Glendale, AZ, USA

Christopher P. Heesy Dept. of Anatomy, Midwestern Univ., Glendale, AZ, USA

Sönke Johnsen Biology Dept., Duke Univ., Durham, NC, USA

Thomas J. Lisney Dept. of Psychology, Univ. of Alberta, Edmonton, AB, Canada

Ellis R. Loew Dept. of Biomedical Sciences, Cornell Univ., Ithaca, NY, USA

Gillian Moritz Dept. of Anthropology, Dartmouth College, Hanover, NH, USA

Saúl S. Nava Dept. of Molecular & Cellular Biology, Harvard Univ., Cambridge, MA, USA

Eric Warrant Dept. of Biology, Univ. of Lund, Sölvegatan, Lund, Sweden

Kara E. Yopak School of Animal Biology & UWA Oceans Institute, The Univ. of Western Australia, Crawley, WA, Australia

Esteban Fernández-Juricic Dept. of Biological Sciences, Purdue Univ., West Lafayette, IN, USA

Vertebrates possess different types of retinal specializations that vary in number, size, shape, and position in the retina. This diversity in retinal configuration has been revealed through topographic maps, which show variations in neuron density across the retina. Although topographic maps of about 300 vertebrates are available, there is no method for characterizing retinal traits quantitatively. Our goal is to present a novel method to standardize information on the position of the retinal specializations and changes in retinal ganglion cell (RGC) density across the retina from published topographic maps. We measured the position of the retinal specialization using two Cartesian coordinates and the gradient in cell density by sampling ganglion cell density values along four axes (nasal, temporal, ventral, and dorsal). Using this information, along with the peak and lowest RGC densities, we conducted discriminant function analyses (DFAs) to establish if this method is sensitive to distinguish three common types of retinal specializations (fovea, *area*, and visual streak). The discrimination ability of the model was higher when considering terrestrial (78%–80% correct classification) and aquatic (77%–86% correct classification) species separately than together. Our method can be used in the future to test specific hypotheses on the differences in retinal morphology between retinal specializations and the association between retinal morphology and behavioral and ecological traits using comparative methods controlling for phylogenetic effects.

Keywords: fovea, ganglion cells, retina, topographic maps, visual ecology, visual streak

Citation: Moore, B. A., Kamilar, J. M., Collin, S. P., Bininda-Emonds, O. R. P., Dominy, N. J., Hall, M. I., et al. (2012). A novel method for comparative analysis of retinal specialization traits from topographic maps. *Journal of Vision*, *12*(12):13, 1–24, http://www.journalofvision.org/content/12/12/13, doi:10.1167/12.12.13.

doi: 10.1167/12.12.13 Received October 6, 2011; published November 20, 2012 ISSN 1534-7362 © 2012 ARVO

Downloaded from jov.arvojournals.org on 07/19/2019

Introduction

The vertebrate retina is a thin layer of neural tissue lining the back of the eye that samples visual information from the environment before it reaches the visual centers of the brain. Photoreceptor cells are responsible for absorbing light energy or photons and transforming these into electrical signals that pass through a series of interneurons (bipolar, amacrine, and horizontal cells) before reaching the retinal ganglion cells (RGCs), whose axons form the optic nerve. The optic nerve is organized so that retinotopic information processed at the level of the retina is carried to specific regions of the central nervous system (McIlwain, 1996). The density of photoreceptors and RGCs is not homogeneous across the retina (Bozzano & Collin, 2000; Hughes, 1977; Schiviz, Ruf, Kuebber-Heiss, Schubert, & Ahnelt, 2008; Wagner, Frohlich, Negishi, & Collin, 1998; Walls, 1942). Regions of the retina with a higher density of photoreceptors and RGCs are known as retinal specializations (Meyer, 1977; Walls, 1942). These specializations provide higher spatial resolving power in discrete regions of the visual field (Collin, 1999). Therefore, animals rely on these specializations to obtain high quality information about their environment.

Across vertebrates, different types of retinal specializations have been identified, such as foveae, *areae*, and visual streaks, each varying in number, size, shape, and position in the retina (Collin, 1999; Collin & Shand, 2003; Hughes, 1977; Walls, 1942). A fovea is a pitted invagination of retinal tissue with a high density of photoreceptors and is surrounded by high densities of RGCs, where the inner retinal layers are displaced and the elongated photoreceptors attain their highest level of cell packing. The fovea is considered to mediate the highest spatial resolving power of all retinal specializations (Inzunza, Bravo, & Smith, 1989; Ross, 2004). An *area* is a concentric increase in ganglion cell or photoreceptor density, but without any obvious retinal displacement of the retinal layers. A visual streak is a band-like *area* extending horizontally across the retina allowing higher spatial sampling of a panoramic visual field. Each species possesses a specific arrangement of retinal specializations, which appears to be under selective pressure by virtue of its ecological niche, ambient light conditions, and habitat complexity (Collin, 1999).

Studying the distribution of neurons across the retina, or retinal topography, of a given species can help us understand how organisms visually perceive their environment, which ultimately affects their behavior (Fernández-Juricic, Gall, et al., 2011; Temple, Hart, Marshall, & Collin, 2010). For instance, among falconiform birds, predatory species have been shown to possess both central and temporal foveae, whereas the carrion-eating species have a single central fovea (Inzunza, Bravo, Smith, & Angel, 1991). Differences in the location of the retinal specializations in these species may be related to foraging strategies: predatory species are involved in more visually demanding tasks than carrion-eating species, which could account for the presence of the second foveae (Inzunza et al., 1991).

The comparative assessment of the diversity in retinal topography has important implications for better understanding the adaptations of the vertebrate visual system to different environmental conditions. This is particularly relevant given the large number of species whose retinal topography has been examined. Collin (2008) collated published topographic maps and released a public archive (see http://www.retinalmaps.com.au/) with over 300 species of vertebrates and over 1,000 maps. Despite some studies characterizing cell density gradients across the retina (Wässle & Boycott, 1991; Wässle, Grünert, Röhrenbeck, & Boycott, 1989), at present there is no single standard method for measuring retinal specialization traits quantitatively, such as type, position, and changes in cell density from the retinal periphery to the center of different retinal specializations. Such a capability would harness the power of this large comparative resource and allow us to test more challenging hypotheses regarding the evolution of vision across vertebrate taxa.

The aim of this study is to present a novel method to quantify the position of the retinal specialization and the concomitant changes in cell density across the retina. Additionally, using a commonly used statistical tool (discriminant function analysis [DFA]), we determined whether traits obtained by our method (retinal specialization position and cell density gradients) in combination with other retinal traits (peak and lowest ganglion cell densities) would be sensitive enough to distinguish among three common types of retinal specializations (fovea, *area*, or visual streak) in terrestrial and aquatic vertebrates. The methodological procedures presented in this study will have wide applicability in a comparative context by allowing us to standardize the measurement of retinal features from already published topographic maps in species with different eye size, orbit position in the skull, and overall retinal cell density.

Methods

This section is divided in three main parts. First, we describe the database on topographic maps gathered for this study. Second, we explain in detail the novel method we used to collect information on retinal specialization position, ganglion cell density gradients, and peak and lowest cell densities from topographic

Downloaded from jov.arvojournals.org on 07/19/2019

maps. Finally, we test our method by incorporating these retinal parameters into a DFA to test whether they can classify the topographic maps correctly into different types of retinal specializations (fovea, *area*, or visual streak).

Topographic maps database

We used published topographic maps of the RGC layer instead of the photoreceptor layer because they are more readily available in the literature. The original data consisted of counts of RGCs in different regions of the retina that were used to build the topographic maps. Most of the maps used in this study are available in the retinal topographic map database: http://www.retinalmaps.com.au/ (Collin, 2008). We used topographic maps from 88 species of vertebrates (Chondrichthyes, 6; Actinopterygii, 25; Amphibia, 1; "Reptilia," 2; Aves, 21; Mammalia, 33; Appendix 1). Within Mammalia, we did not use the published topographic maps of the human retina (Curcio & Allen, 1990; Harman, Abrahams, Moore, & Hoskins, 2000), as they were not technically compatible with our methods. In the text, we used the common names of the species, but scientific names are available in Appendix 1. We classified species as aquatic if part of their life cycle relied on water for foraging and/or breeding purposes. Otherwise, species were considered terrestrial (Appendix 1).

We chose topographic maps that provided the orientation and scale of the retina with easily distinguished and properly labeled iso-density lines. We classified retinal specializations into three categories (fovea, *area*, and visual streak) based on the descriptions and topographic maps presented in the original published papers and some specific criteria (details in Appendix 2). In a limited number of studies, more than one map per species was available, and we chose the one the authors deemed most representative. The topographic map of each species was taken as the unit upon which we made measurements on different retinal traits (see below).

From the topographic maps (see example in Figure 1a), we quantified eight traits: (1–2) position of the retinal specialization with two coordinates, (3–6) changes in ganglion cell density from the retinal periphery to the center of the retinal specialization (cell density gradient) in four different regions of the retina (nasal, temporal, dorsal, and ventral), (7) peak RGC density, and (8) lowest RGC density. The position of the retinal specialization is relevant to establish the projection of the area with the highest spatial resolving power into the visual field (Collin, 1999). For instance, in a species with laterally-placed eyes, a temporal retinal specialization will project into the binocular visual field. The ganglion cell density gradient from the retinal periphery to the center of the retinal specialization varies substantially between species (Dolan & Fernández-Juricic, 2010). This cell density gradient is a proxy for how improved spatial resolving power provided by the retinal specialization is compared to the retinal periphery (Fernández-Juricic, Moore, et al., 2011). For instance, species with a steep cell density gradient are expected to rely more on the retinal specialization for visualizing objects, which could in turn affect patterns of visual search and visual fixation (Fernández-Juricic, Moore, et al., 2011). Finally, the highest and lowest RGC densities are proxies for the maximum and minimum levels, respectively, of spatial resolving power within the retina. The peak RGC density has been used in the calculation of the upper levels of visual acuity in some species (Boire, Dufour, Theoret, & Ptito, 2001; Collin & Pettigrew, 1989; Dolan & Fernández-Juricic, 2010; Hughes, 1977; Pettigrew et al., 1988).

Retinal parameters

Position of the retinal specialization

We first established the location of the *center* of the retinal specialization in the topographic map. For a fovea, given its relatively small size, the position was generally marked in the topographic map as a point. The fovea can be identified from a wholemounted retina as a circular pit on the retinal tissue. However, the *area* and the visual streak occupy a relatively larger spatial extent than the fovea (Walls, 1937). Therefore, we determined the center of either type of retinal specialization as the point with the highest cell density identified in each published topographic map. If this point was not reported, we marked it as the middle point within the highest cell density range because the highest cell density is usually located at the center of the upper cell density range in most topographic maps (Collin, 2008).

To quantify the position of the retinal specialization, we used a Cartesian coordinate system (see also Mastronade, Thibeault, & Dubin, 1984). Because the outer edges of the retina are removed in a nonuniform fashion during the retinal wholemounting process (Stone, 1981; Ullmann, Moore, Temple, Fernández-Juricic, & Collin, 2012; Figure 1a), we fitted a circle over the retina by eye based on two criteria: the circle encompassed as much of the retina as possible, and the gaps between the circle and the periphery of the retina were minimized (Figure 1b). Once the circle was fitted over the retina, we determined the center of the circle as the intersection of any two diameters, which were traced with Autocad 2010 (Autodesk, San Rafael, CA, USA, http://usa.autodesk.com/autocad/).

Downloaded from jov.arvojournals.org on 07/19/2019

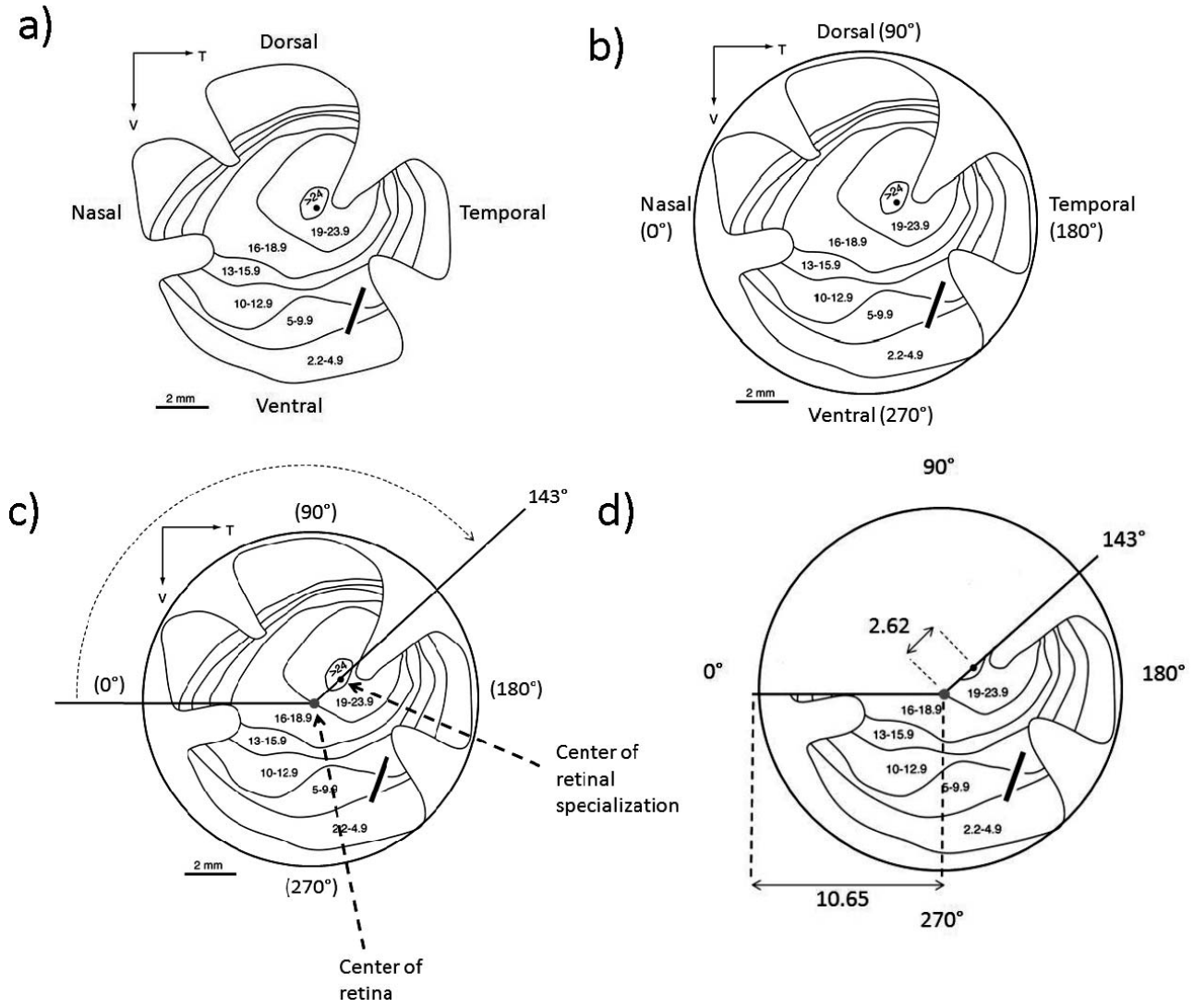

Figure 1. (a) Topographic map of the retinal ganglion cell distribution of the California Towhee *Pipilo crissalis* (Fernández-Juricic, Gall, et al., 2011). Shown are iso-density lines (connecting areas of the retina with the same cell density). (b) Circle fitting of the edges of the retina. (c) Angle between the center of the retinal specialization and the nasal axis of the retina. The gray dot represents the center of the retina and the black dot, the center of the retinal specialization. (d) Distance from the center of the retina to the center of the retinal specialization (2.62). This distance is divided by the radius of the circle (10.65) to obtain a standardized distance of the retinal specialization to the center of the retina (0.25).

From the center of the retina, we then measured the angle of the retinal specialization (in degrees, Θ). The nasal part of the retina was considered as 0° for both right and left eyes, which allowed us to standardize measurements across species irrespective of the eye used to generate the topographic map. We then established 90° as dorsal, 180° as temporal, and 270° as ventral (Figure 1b). The angle of the retinal specialization was measured in relation to the nasal direction (Figure 1c). We measured the relative distance from the center of the retina to the center of the retinal specialization. We first drew a line from the center point of the retina to the retinal specialization (Figure 1d) and measured this distance with the aligned measurement tool in Autocad 2010 (Figure 1d). We divided this distance by the radius of the circle to obtain a standardized distance (Figure 1d), which varied from 0 to 1.

We converted the angle of the retinal specialization (Θ) and its distance to the center of the retina (r) into Cartesian coordinates, which are both linear (x and y) and can be any positive or negative number (Figure 2). We used $(r)\cos\Theta$ to obtain the x-coordinate and $(r)\sin\Theta$ to obtain the y-coordinate. Cartesian coordinates consist of two linear positive and/or negative values; thus, a right and left retina will provide different x-coordinate values since the eye is flipped around the y-axis. To maintain consistency, we made right eyes the

Downloaded from jov.arvojournals.org on 07/19/2019

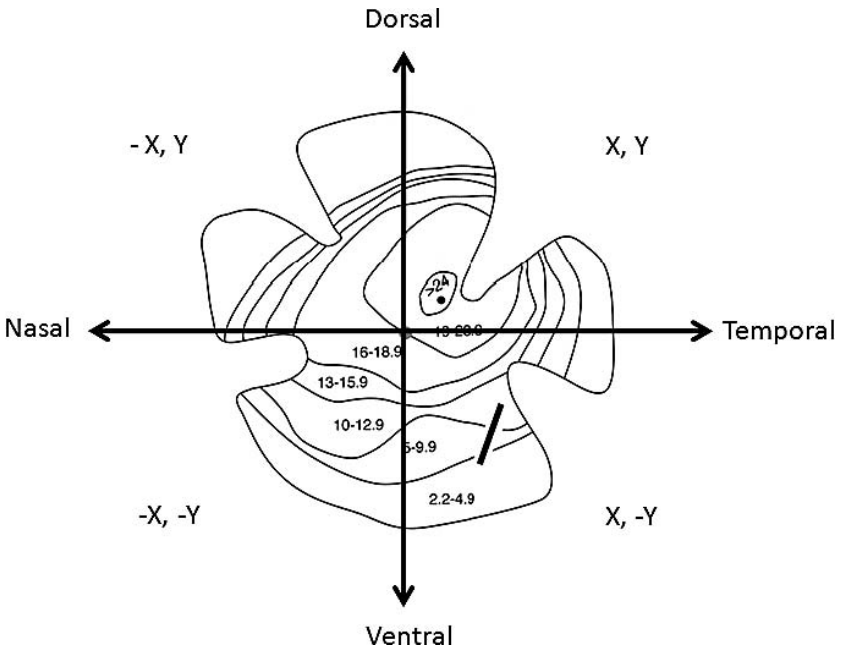

Figure 2. Cartesian coordinates to establish the position of the retinal specialization in the retina. The coordinates consist of two linear distances (*x*- and *y*-coordinates) of both positive and negative values, depending on whether the position of the specialization is on the dorsal, ventral, nasal, or temporal sides of the retina.

standard, inversing the sign of the *x*-coordinate for left eyes. Using Cartesian coordinates assumes that the wholemounting process was done similarly across studies to produce the topographic maps. However, this is unlikely to be the case, which could introduce a certain degree of error in our measurements (see more details in the Discussion).

Cell density gradient across the retina

Topographic maps provide a visual representation of variations in cell density across the retina using lines (iso-density lines or contours, Figure 1a) that connect areas of the retina with similar density (Stone, 1981; Ullmann et al., 2012). We used these iso-density lines and the regions in the retina they delimit to establish changes in cell density from the retinal periphery to the retinal specialization. We used the center of the retinal specialization (see above) as a reference point to draw four vectors across the retina in the nasal, dorsal, temporal, and ventral directions using Microsoft Powerpoint© (Figure 3a). Using Image J (Rasband, 1997–2012), we scaled the topographic map based on the scale provided in the original publication. Along each of the four vectors (dorsal, temporal, ventral, and nasal), we marked the points where iso-density lines would intersect with each vector (Figure 3a). In some topographic maps, the vectors would lie on a radial cut of the retina (originally made to flatten the retina onto the slide during the wholemounting procedure). In these instances, we projected the iso-density line into the void space from each direction, taking into consideration the normal curvature of the retina.

We set sampling points along two pairs of vectors (nasal-temporal and dorsal-ventral; Figure 3a and b). Along each pair of vectors, we established 21 evenly-spaced sampling points (Figure 3b shows an example with the nasal-temporal vector), with the first and last sampling point marking the edges of the retina, yielding 20 evenly-spaced intervals (Figures 3b and 4d). At each of the 21 sampling points, the average density of RGCs was recorded by determining which iso-density lines each sampling point fell into (i.e., between which iso-density lines; Figure 4a through f).

First, we measured the distance (mm) between iso-density lines along a given vector (nasal-temporal and dorsal-ventral; Figure 4b). Second, we measured the cumulative distance (mm) at each iso-density line (Figure 4c). Third, we determined the distance (mm) between each sampling point along the vector by multiplying the total length of the vector (e.g., 12.28 mm in Figure 4) by 0.05 (e.g., 0.614 mm in Figure 4) to establish 21 sampling points that were equidistant to each other (Figure 4d). Fourth, we calculated the cumulative distances across sampling points along a given vector (Figure 4e). Fifth, if the cumulative distance up to a particular sampling point was smaller than the cumulative distance up to the iso-density line with the next higher cell density value, we established the mean RGC density for that particular sampling point to be the averaged density between the upper and lower cell density ranges bounded by the iso-density

Downloaded from jov.arvojournals.org on 07/19/2019

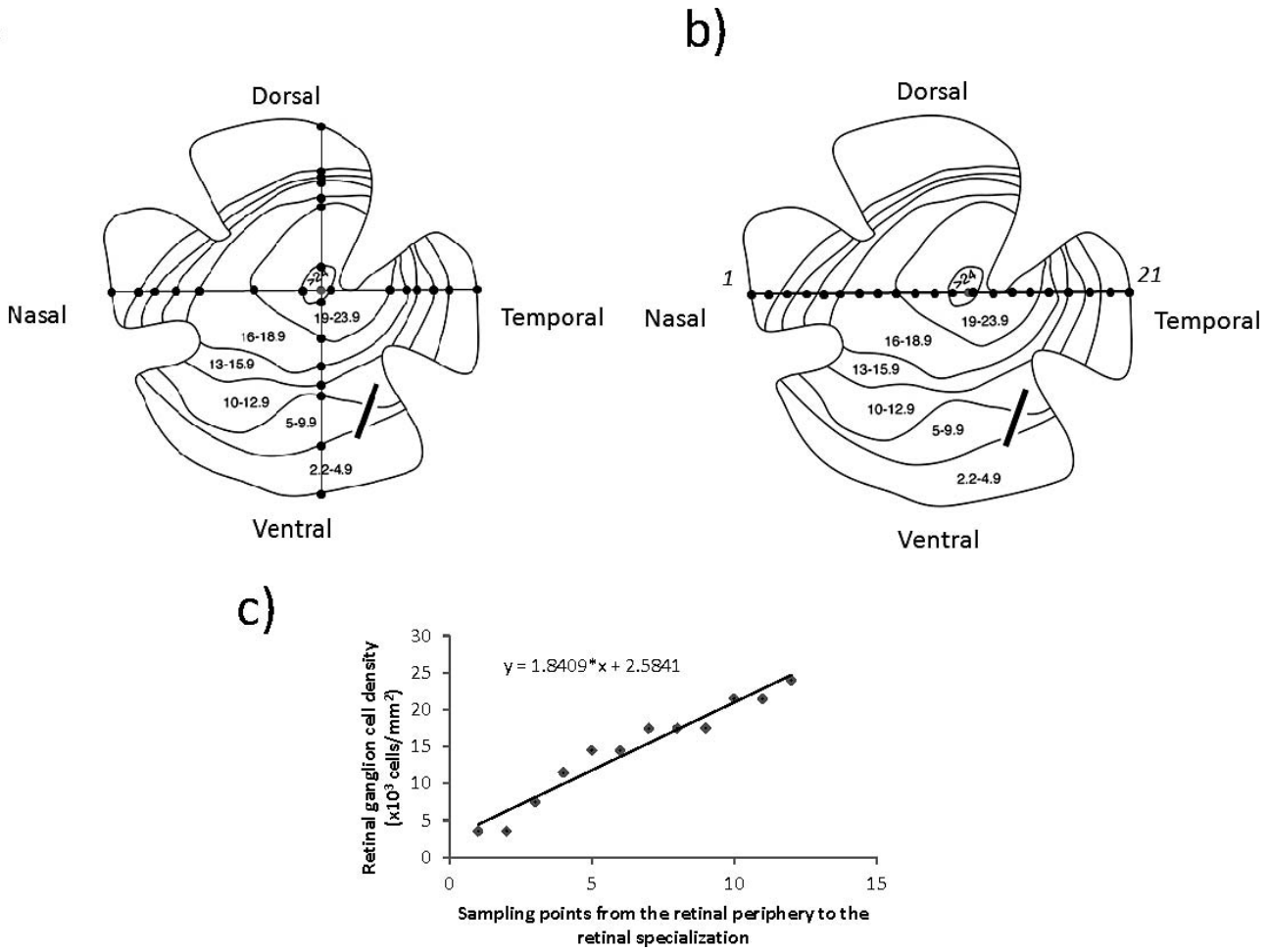

Figure 3. (a) Example of the cell density points at the intersection of the iso-density lines along the nasal-temporal and dorsal-ventral vectors crossing the center of the retinal specialization. Notice that the line extends into the radial cuts of the retina (see text for details). (b) Example of the 21 cell density sampling points along the nasal-temporal vector, which divided the sampling line into 20 even spaces. At each point, we measured the mean cell density value that it fell in. (c) Example of the plot of the mean cell density in each sampling point from the temporal periphery of the retina to the center of the retinal specialization. We fitted a line and used its slope as the rate of change in cell density from the retinal periphery to the retinal specialization.

lines that the sampling point fell into (Figure 4f). For instance, in Figure 4, the cumulative distance up to sampling point 3 is 1.228 mm (Figure 4e), which is smaller than the cumulative distance up to the proceeding iso-density line 4, 1.841 mm, with a higher cell density value (Figure 4e). Therefore, the final cell density value obtained for sampling plot 3 was estimated to be 7,500 cells/mm^2 (i.e., average of the cell density range 5,000–9,900 cells/mm^2; Figure 4f). We followed the same procedure to estimate the cell densities of all other sampling points, which were used for the calculation of the slope.

The number of sampling points (21) along a given vector allowed us to capture the high diversity in iso-density line configurations present in the published topographic maps used in this study. We tried using fewer sampling points, but missed changes in iso-density categories in some of the topographic maps. In some cases, some of the 21 sampling points did not fall within the peak density range of the retinal specialization. To determine whether or not this caused a significant change in our slope estimates, we increased the number of sampling points to include the cell density range of the retinal specialization and recalculated the slope. We found that these two measurements were highly correlated (nasal, $r = 0.99$, $p < 0.001$; temporal, $r = 0.96$, $p < 0.001$; dorsal, $r = 0.99$, $p < 0.001$; ventral, $r = 0.99$, $p < 0.001$). Consequently, we decided to use the 21 sampling points to be consistent across all topographic maps.

In some cases, the published topographic maps did not include the RGC density for the outer perimeter of the retina. For these maps, when a sampling point fell into the peripheral cell density range, we established that the cell density would be half of the density of the first iso-density line shown nearest the periphery, based

Downloaded from jov.arvojournals.org on 07/19/2019

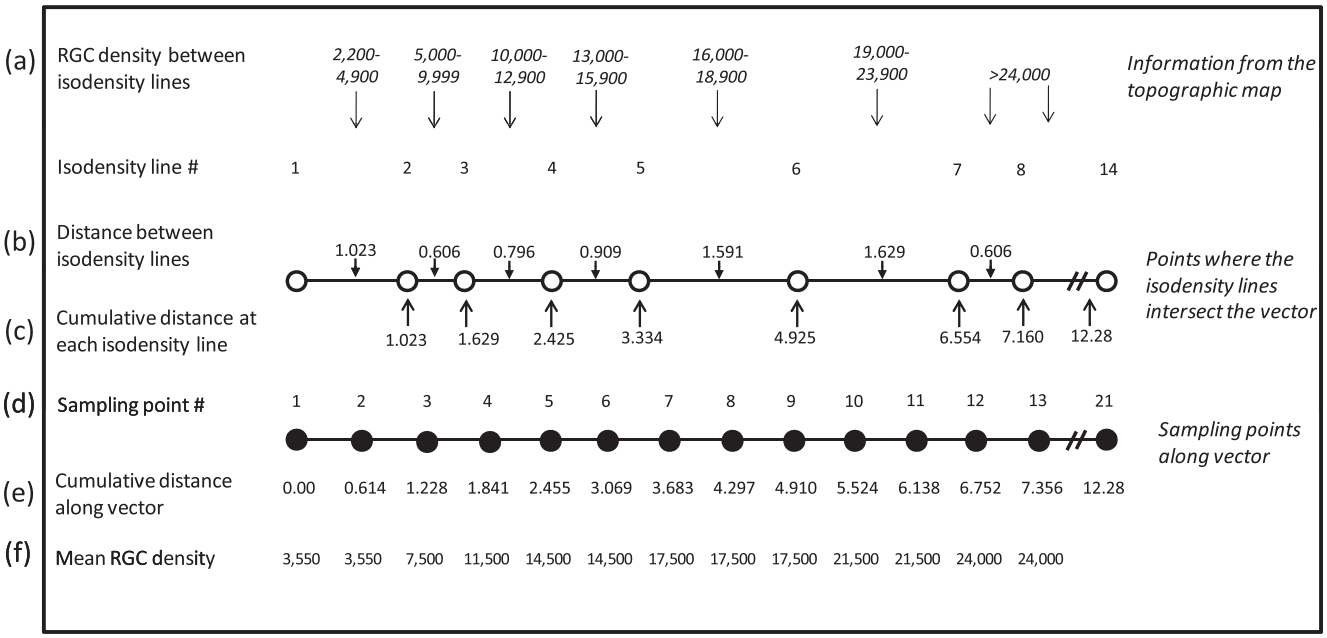

Figure 4. Example of how to determine the mean cell density for each of the 21 sampling points. Shown are the first 13 and the last sampling points for the sake of clarity. Distances were scaled to mm to fit the scale provided in the topographic maps. Open circles represent the iso-density lines, and solid circles are the evenly spaced sampling points. The mean RGC density is an average of the RGC range between two iso-density lines. The edges of the retina are marked with sampling point 1 (0.00 mm) and 21 (12.28 mm). Sampling point 13 is the point that falls along the vector prior to crossing over the peak cell density of the retinal specialization. See explanation of the different steps (a through f) in the text.

on patterns observed in maps that included this piece of information. For instance, if the first peripheral iso-density value was 500 cells/mm^2, a sampling point falling into this range would have a ganglion cell density value of 250 cells/mm^2. After the RGC density values had been recorded for all 21 points on the pairs of vectors (nasal-temporal and dorsal-ventral), we split them into four separate vectors (nasal, temporal, ventral, and dorsal). We then plotted the mean RGC density values at each sampling point and fitted the changes in cell density across the retina with a linear and nonlinear functions (second order polynomial). From the linear fitting, we used the slope of that line as a proxy for the gradient in cell density change from the retinal periphery to the retinal specialization (example in Figure 3c). From the nonlinear fitting, we used the coefficients of the first and second order polynomials as the proxies for the gradient in cell density change. We also ran the analyses with a third order polynomial (data not shown; results available from the corresponding author), but the fit was even worse than the linear and second order polynomial. We took this dual approach (linear and nonlinear) in the cell density gradient characterization since some of the gradients deviated from linearity.

For instance, in some topographic maps (pigmented rabbit, black bream, painted flutemouth, spookfish, and staghorn damselfish), we could only get two different cell density values on a specific retinal direction (e.g., a plateau followed by a sudden increase in cell density) because of the low number of iso-density categories or because the retinal specialization was too close to the edge of the retina, reducing the number of sampling points on that specific direction of the retina. For the linear approach, we fitted the data with a Multivariate Adaptive Regression Splines (MARSplines) analysis, which yielded a weighted slope based on slopes from lines fitted to different parts of the relationship based on differences in the coefficient of determination (Statsoft, 2012). The slope values obtained from the MARSplines analysis were similar to those obtained through linear regression fitting. Therefore, we decided to use the latter so that the slope values were comparable across species. Using a similar procedure for all taxa is particularly important for the application of our method in comparative analyses. Finally, the gradient in cell density change in the nasal regions of the great kiskadee, coral cod, carangid fish, small dogfish, and softskin smoothhead showed a pattern of increasing-decreasing-increasing cell density from the retinal periphery to the center of the retinal specialization. To determine if the slopes of cell density change on a single retinal direction of these species would bias the conclusions of the linear approach, we reran our statistical analysis classifying retinal specializations based on the studied traits (DFA, see below) excluding

Downloaded from jov.arvojournals.org on 07/19/2019

these species, but the overall classification scores were very similar to the analysis including these species (available from the corresponding author upon request). We therefore included these five species in the analyses to assess the discrimination ability of the model based on a wide range of retinal topographic configurations.

Peak and lowest cell density

From the original publications and the topographic maps, we obtained the peak RGC density. The lowest cell density was obtained from the topographic maps as the cell density at the periphery of the retina. In some cases, the cell density at the periphery was not available. We then established the cell density as half of the density of the first iso-density line reported in the topographic map (see below).

Statistical analysis

The analysis included measurements from 26 foveae, 35 visual streaks, and 33 *areae*. Six species were represented twice in our dataset (Appendix 1) due to the presence of two retinal specializations in different regions of their retinas: Chilean eagle and American kestrel (central and temporal foveae), and rock pigeon, great kiskadee, and rusty-marginated flycatcher (central fovea and *area temporalis*), and harlequin tuskfish (streak and *area*). We decided to include the second retinal specialization from each of these species due to the different morphologies within each retina (e.g., the central retinal specialization had a higher cell density than the temporal) and to determine if our method could tell the two types of specializations apart on a given species. However, we acknowledge that this introduced a bias by having two data points from each of these six species. We justified this on the basis that this study focuses on presenting a novel method rather than analyzing retinal configurations from a comparative perspective controlling for the effects of phylogenetic relatedness.

We used a DFA (Huberty, 1994; Quinn & Keough, 2002) to assess the ability of our method to assign the different topographic maps to three types of retinal specializations (fovea, *area*, and visual streak). We chose the DFA over other classification techniques (e.g., artificial neural networks) because its results are easier to interpret. We included in the DFA the eight retinal traits studied for each topographic map, along with the type of retinal specialization. The DFA generated canonical discriminant functions based on the linear combinations of the eight retinal traits maximizing the probability of correctly assigning cases (e.g., topographic maps) to specific categories (e.g., type of retinal specialization; Huberty, 1994). The DFA used the relative sizes of the standardized coefficients of each discriminant function (Huberty, 1994) to establish the retinal traits that best discriminated among types of retinal specializations. By solving the discriminant functions, the DFA estimated discriminant function scores for each topographic map on each function (Quinn & Keough, 2002). This information was used in a canonical correlation analysis to plot the values of each topographic map along the roots (i.e., eigenvalues associated with the respective discriminant function; Statsoft, 2012) to assess visually the degree to which observations belonging to different types of retinal specializations grouped together (e.g., Figures 5 and 6 show the roots of the canonical analysis). Additionally, the DFA derived a classification equation for each type of retinal specialization (Quinn & Keough, 2002), which was used to estimate a classification score for each topographic map. Then each topographic map was assigned to the type of retinal specialization based on its classification score, which allowed the DFA to estimate the percentage of observations that were correctly classified (Quinn & Keough, 2002). The DFA shares assumptions with general linear models (Tabachnick & Fidell, 1996).

For the DFA, we used Wilks' Lambda as the test statistic, which was then used to estimate an F statistic and p-value. Given that some of the traits we measured had a high degree of correlation (>0.70; peak RGC density and nasal, dorsal, and ventral gradient in cell density), we used a forward stepwise selection method to enter the traits in the model. This model selection procedure enhanced the classification score of the DFA in comparison to standard selection procedures forcing all traits into the model. In the DFA, we used a-priori classification probabilities that were proportional to group sizes (Statsoft, 2012). We first ran the DFA model, pooling terrestrial and aquatic species together, and then considered them separately due to potential differences in retinal configuration (Mass & Supin, 2007). We ran two sets of DFA models, one for the linear and one for the nonlinear approach. For the DFA using the linear approach, we included the following parameters: peak RGC density, lowest RGC density, x-coordinate position, y-coordinate position, and nasal, temporal, dorsal, and ventral slopes. For the DFA using the nonlinear approach, we had two slope coefficients (first and second order polynomials) in each of the four retinal directions. Because these coefficients are not independent of each other, we ran a principal component analysis (PCA) to combine the two coefficients into a single factor before running the DFA models. Thus, for the DFA using the nonlinear approach, we included the following parameters: peak RGC density, lowest RGC density, x-coordinate position, y-coordinate position, nasal PCA

Downloaded from jov.arvojournals.org on 07/19/2019

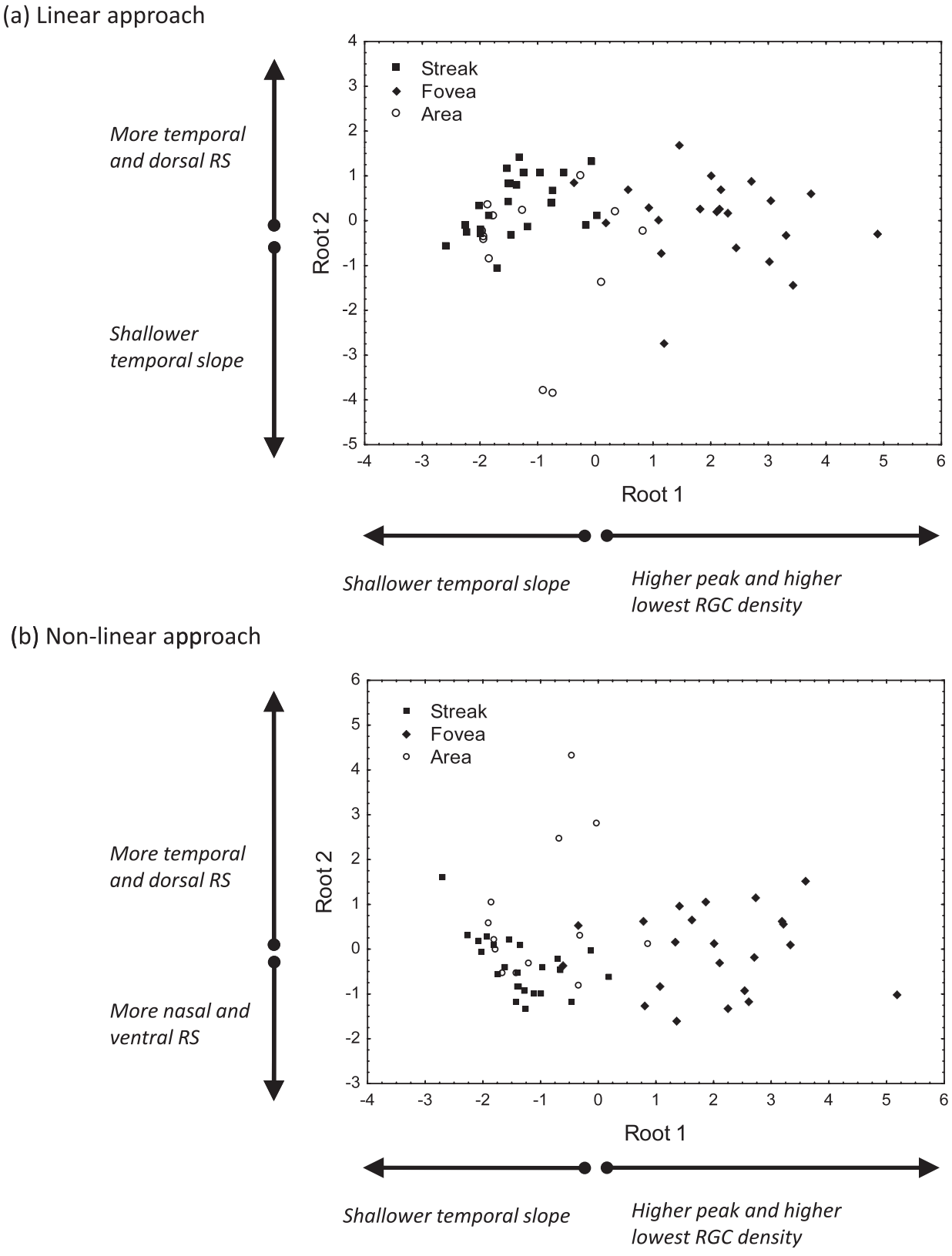

Figure 5. Scatterplot of the discriminant functions (canonical axis scores) showing the discrimination of the three types of retinal specializations (fovea, area, and visual streak) for terrestrial vertebrates. We used two approaches, (a) linear and (b) nonlinear, to quantify cell density gradients (details in the text). Only two canonical axis scores were computed in each case. RS, retinal specialization.

Downloaded from jov.arvojournals.org on 07/19/2019

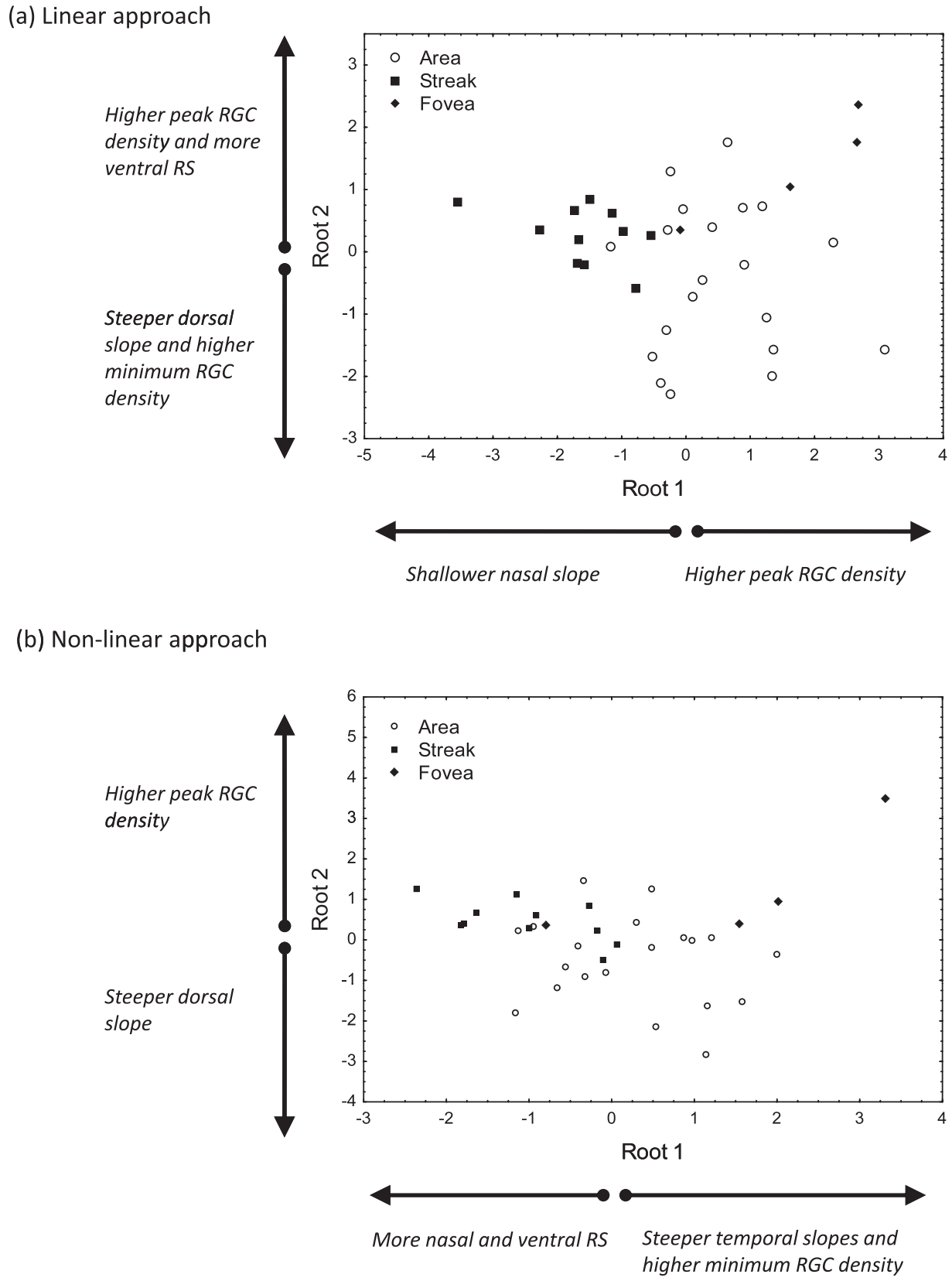

Figure 6. Scatterplot of the discriminant functions (canonical axis scores) showing the discrimination of the three types of retinal specializations (fovea, area, and visual streak) for aquatic vertebrates. We used two approaches, (a) linear and (b) nonlinear, to quantify cell density gradients (details in the text). Only two canonical axis scores were computed in each case. RS, retinal specialization.

Downloaded from jov.arvojournals.org on 07/19/2019

	Mean ± *SD*	Min.	Species with min.	Max.	Species with max.
Lowest retinal ganglion cell (RGC) density	2,340.1 ± 276.7 (116)	10	Western gray kangaroo	12,000	Brown-headed cowbird
Peak RGC density	21,684.9 ± 1947.8 (88)	220	Koala	65,000	American kestrel
Nasal slope	1.05 ± 0.12 (111)	0.007	African elephant	5.77	Rusty-marginated Flycatcher
Temporal slope	2.59 ± 0.37 (140)	0.015	Koala	20.00	Painted flutemouth
Dorsal slope	1.55 ± 0.21 (132)	0.004	Koala	10.50	Rock pigeon
Ventral slope	1.51 ± 0.18 (116)	0.021	Western gray kangaroo	10.00	Staghorn damselfish
x-coordinate	0.01 ± 0.04 (2686)	−0.761	Shovelnose ray	0.81	Painted flutemouth
y-coordinate	−0.03 ± 0.02 (710)	−0.809	Spookfish	0.64	Black bream

Table 1. Descriptive statistics on the different retinal traits measured from the topographic maps of 88 species of vertebrates (see text for details). Values within parentheses are coefficients of variation.

factor, temporal PCA factor, dorsal PCA factor, and ventral PCA factor. Therefore, the DFA models using the linear and nonlinear approaches included the same number of parameters.

Results

We obtained measurements on all the retinal traits from 94 topographic maps belonging to 88 species of vertebrates (Table 1). Based on the coefficients of variation, position in the *x*- and *y*-coordinates showed the highest degree of variability between species, whereas peak RGC density and nasal gradient in cell density showed the lowest (Table 1). Different taxa were represented in the extreme values of the traits measured. The minimum values of the lowest and highest RGC density and cell density gradient in all regions of the retina were represented by mammals, and the minimum values of the *x*- and *y*-coordinate were represented by cartilaginous and ray-finned fishes (Actinopterygii and Chondrichthyes; Table 1). The maximum values of lowest and peak RGC density gradients and nasal, temporal, and ventral gradients in cell density were represented by birds, whereas the maximum values of the dorsal gradient in cell density and *x*- and *y*-coordinates were represented by ray-finned fish (Actinopterygii; Table 1).

Considering all species, the DFA with a linear approach selected five factors out of the eight: nasal and dorsal gradients in cell density, lowest RGC density, and *x*- and *y*-coordinate positions of the retinal specialization. With these factors, the DFA significantly discriminated among the three retinal specializations, $F(10, 174) = 6.37$, $p < 0.001$. This DFA correctly classified 66% of the retinal specializations to the correct type. The visual streak (28 out of 35, 80%) and the fovea (16 out of 26, 61.5%) had the highest classification scores, whereas the *area* (18 out of 33, 54.6%) had the lowest. The DFA with a nonlinear approach selected six factors that yielded a significant discrimination among retinal specializations, $F(12, 172) = 5.24$, $p < 0.001$: nasal, dorsal, and ventral PCA factors representing the gradients in cell density, lowest RGC density, and *x*- and *y*-coordinate positions of the retinal specialization. The DFA with a nonlinear approach correctly classified 67% of the retinal specializations to the correct type. The visual streak (30 out of 35, 85.7%) had the highest classification scores, followed by the fovea (15 out of 26, 57.7%) and the *area* (18 out of 33, 54.6%). Models with both approaches (linear and nonlinear) performed at similar levels.

We found that sorting species out into terrestrial versus aquatic increased the overall classification scores of the DFA models. Considering terrestrial species, five factors were selected by the DFA with a linear approach to discriminate significantly among the retinal specializations, $F(10, 104) = 11.18$, $p < 0.001$: peak and lowest RGC densities, temporal gradient in cell density, *x*- and *y*-coordinate positions of the retinal specialization. This DFA model increased the overall classification score of the 59 topographic maps of terrestrial species to 77.97%. The visual streak (23 out of 24, 95.8%) and the fovea (20 out of 22, 90.9%) had the highest classification scores, whereas the *area* (3 out of 13, 23.1%), the lowest. In nine mammal species, the *area* was misclassified as a visual streak (Table 2). The DFA with a nonlinear approach for terrestrial species also discriminated significantly among retinal specializations, $F(12, 102) = 9.11$, $p < 0.001$, including six factors: peak and lowest RGC densities, *x*- and *y*-coordinate positions of the retinal specialization, and dorsal and temporal PCA factors representing the gradients in cell density. The overall classification score of this DFA was 79.7%, with the visual streak (23 out of 24, 95.8%) and the fovea (20 out of 22, 90.9%) having the highest scores, and the *area* the lowest (4 out of 13, 30.77%). In eight mammal species, the visual streak was misclassified (Table 2). Models with both approaches (linear and nonlinear) for terrestrial species performed at similar levels.

Downloaded from jov.arvojournals.org on 07/19/2019

Species common name	Type of RS	Misclassified using the linear approach as	Misclassified using the nonlinear approach as
Peafowl	*area*	fovea	fovea
Mouse lemur	*area*	visual streak	visual streak
Tree kangaroo	*area*	visual streak	visual streak
North American opossum	*area*	visual streak	visual streak
Three-toed sloth	*area*	visual streak	N/A
Golden hamster	*area*	visual streak	visual streak
Ferret	*area*	visual streak	visual streak
Galago	*area*	visual streak	visual streak
Koala	*area*	visual streak	visual streak
Hooded rat	*area*	visual streak	visual streak
Anubis baboon	fovea	visual streak	*area*
Owl monkey	fovea	visual streak	visual streak
Beagle	visual streak	*area*	*area*

Table 2. Topographic maps of terrestrial vertebrates that were misclassified by the DFAs considering different retinal traits (see text for details). Two approaches were used (linear and nonlinear) for the classification. Scientific names are presented in Appendix 1. RS, retinal specialization.

The plots of the first and second canonical axis scores (roots 1 and 2 in Figure 5) of the terrestrial species for both the linear and nonlinear approaches for quantifying cell density gradients show that there is little overlap between the fovea and the visual streak (Figure 5a and b), which were discriminated mostly along the first canonical axis scores (root 1). Based on the factors with the higher loadings on the canonical axes, species with a fovea showed higher peak and lowest RGC density, whereas species with a visual streak showed a shallower temporal gradient in cell density. The *area* had intermediate values along root 1 (Figure 5a and b). With respect to the second canonical axis scores (root 2 in Figure 5), a slightly larger number of species with foveae and visual streaks had their retinal specialization located in the dorsal and temporal areas of the retina (Figure 5a and b). The main difference between the linear and nonlinear approaches was the bottom-left corner of the plot of the canonical axis scores. In the linear approach, this sector corresponded to species exhibiting shallow temporal gradients in cell density between the retinal periphery and the retinal specialization (Figure 5a), whereas in the nonlinear approach, this sector corresponded to species with more nasal and ventral retinal specializations (Figure 5b). Overall, the *area* overlapped more with the visual streak than with the fovea (Figure 5).

When considering only the aquatic species, seven factors were selected by the DFA with the linear approach for quantifying cell density gradients to discriminate significantly among the retinal specializations, $F(14, 52) = 3.06$, $p = 0.002$: x- and y-coordinate positions of the retinal specialization, peak and lowest RGC densities, and temporal, nasal, and dorsal gradients in cell density. This DFA model assigned 85.7% of the topographic maps to the correct type of retinal specialization (Appendix 2). The *area* had the highest classification scores (18 out of 20, 9%), whereas the visual streak (9 out of 11, 81.8%) and the fovea (3 out of 4, 75%) had the lowest classification scores. In this DFA model, the most common misclassifications were visual streaks that were sorted as *areae* in two fish species (Table 3). The DFA model with the nonlinear approach discriminated significantly among the three retinal specializations, $F(12, 54) = 9.11$, $p < 0.001$. This model included six factors: peak and lowest RGC densities, x- and y-coordinate positions of the retinal specialization, and dorsal and temporal PCA factors representing the gradients in cell density from the retinal periphery to the retinal specialization. The model classified correctly 77.1% of the cases. The *area* had the highest classification score (17 out of 20, 85%), followed by the visual streak (8 out of 11, 72.7%) and the fovea (2 out of 4, 50%). The visual streak and the *area* were commonly misclassified in five fish species (Table 3). The DFA model with a linear approach for aquatic vertebrates performed better than the model with the nonlinear approach.

The plot of the first and second canonical axis scores (roots 1 and 2 in Figure 6) of the aquatic species shows a clear segregation among the fovea, *area*, and visual streak in the linear and nonlinear approaches (Figure 6), particularly along the first canonical axis (root 1 in Figure 6). Based on the factors with the higher loadings on the canonical axes, foveae had higher peak and minimum RGC densities and steeper temporal slopes. Visual streaks had shallower temporal gradients in cell density, higher peak RGC densities, and the fovea was placed more nasally and temporally. Finally, *areae* showed intermediate values between these extremes (Figure 6a and b). The factors associated with the

Downloaded from jov.arvojournals.org on 07/19/2019

Species common name	Type of RS	Misclassified using the linear approach as	Misclassified using the nonlinear approach as
Florida garfish	visual streak	*area*	*area*
Lemon shark	visual streak	*area*	*area*
Harp seal	*area*	visual streak	visual streak
Coral cod	*area*	fovea	N/A
Searsid	fovea	*area*	N/A
Bigfin pearleye	*area*	N/A	visual streak
Creek chub	*area*	N/A	visual streak
Harlequin tuskfish	visual streak	N/A	*area*
Legless searsid	fovea	N/A	*area*
Searsid	fovea	N/A	visual streak

Table 3. Topographic maps of aquatic vertebrates that were misclassified by the DFAs considering different retinal traits (see text for details). Two approaches were used (linear and nonlinear) for the classification. Scientific names are presented in Appendix 1. RS, retinal specialization.

canonical axes were different between the models with the linear and nonlinear approaches (Figure 6).

Both DFA model approaches yielded classification functions for each type of retinal specialization considering terrestrial and aquatic species (Appendix 3). These functions can be used in the future for the calculation of classification scores for species not used in this analysis to further test the classification ability of the models.

Discussion

We presented a novel method to characterize retinal traits based on topographic maps of the RGC layer. This method estimates the position of the retinal specialization and the gradient in cell density from the retinal periphery towards the retinal specialization in four axes relevant to the visual ecology of the animal. This information was complemented with the peak and lowest ganglion cell densities available from the topographic maps. Our method provides a quantitative way of evaluating changes in retinal specialization traits across species to test in the future different visual ecology hypotheses. We found that our method is sensitive to identifying common types of retinal specializations in terrestrial and aquatic mammals (fovea, *area*, and visual streak), which have been generally distinguished on the basis of size and cross-sections of the area with the highest cell density in the retina (Collin, 1999; Hughes, 1977; Walls, 1942). Furthermore, our method can be used to identify retinal topographies that would support different types of retinal specializations on the same retina.

Traditionally, the position of a retinal specialization has been characterized in discrete categories, such as dorsal, ventro-nasal, central, etc. (Hughes, 1977; Meyer, 1977; Walls, 1942). However, this categorization prevents us from making quantitative estimations that can be used to compare the position of the retinal specialization across species living in different visual environments. Quantitative estimates can allow us to determine more accurately the specific position in the visual field that the retinal specialization projects to, which has important behavioral implications (e.g., foraging, Collin, 1999; anti-predator behavior, Fernández-Juricic, 2012; predator-prey interactions, Cronin, 2005). Our method estimates the position of retinal specializations using a Cartesian system that takes into consideration the angle of the retinal specialization in relation to the nasal direction, as well as the distance between the retinal specialization and the center of the retina. For instance, we found that in terrestrial vertebrates, the fovea and visual streak are located more dorsally and temporally, whereas in aquatic vertebrates, the fovea appears to be more ventrally placed. These trends can be tested in future studies using comparative methods controlling for phylogenetic effects.

Our index of the steepness of the gradient in cell density can offer insight into the degree of spatial resolving power provided by the retinal specialization in relation to that of the retinal periphery (Dolan & Fernández-Juricic, 2010; Whiteside, 1967). We found a trend that suggests that foveae have steeper gradients (and thus a more pronounced change in spatial resolving power) from the retinal specialization to the retinal periphery and higher peak ganglion cell density in relation to *areae* and visual streaks. Future comparative studies should assess whether animals with a steep decline in visual resolution towards the retinal periphery rely more heavily upon the retinal specialization for visualizing objects (Fernández-Juricic, Gall, et al. 2011).

We used linear and nonlinear approaches for classifying different retinal specializations, which overall performed similarly. However, both approaches

Downloaded from jov.arvojournals.org on 07/19/2019

were less successful in discriminating among the three retinal specializations when we combined terrestrial and aquatic species than when we considered these groups separately. This could be related to variations in the retinal configuration beyond the known differences in eye characteristics between terrestrial and aquatic vertebrates (Dral, 1972; Mass & Supin, 2007). Compared to terrestrial species, aquatic species appear to have higher densities and larger RGCs (Mass & Supin, 2010), higher densities of amacrine and neuroglial cells (Mass & Supin, 2000), lower numbers of cone photoreceptors (Peichl, Berhmann, & Kroger, 2001), and a higher maximum number of retinal specializations per retina (Collin, 1999). Many of these differences are also taxa-specific (Collin, 1999). The implication is that future comparative studies on retinal topography should assess terrestrial and aquatic species separately.

In terrestrial species, the DFA provided good discrimination (above 90%) for foveae and visual streaks, but lower discrimination for *areae*. On the contrary, in aquatic species, the linear DFA in particular discriminated *areae* better than foveae and visual streaks. One potential factor is that the retinal specialization type with the lower discrimination in either model was the one with the lowest sample size. Additionally, in terrestrial species, *areae* were generally misclassified as visual streaks, whereas in aquatic species, visual streaks were generally misclassified as *areae*. In three of the terrestrial mammals with a misclassified *area* (golden hamster, ferret, and hooded rat), the topographic maps showed an area where the lower cell density isolines were slightly elongated, which is sometimes referred to in the literature as a "weak" visual streak (Collin & Pettigrew, 1988a, b), although it does not meet the morphological criteria we used for visual streaks (Appendix 2). Finally, some of the authors' original classifications included two types of retinal specializations overlapping (e.g., *area* and visual streak). We chose one based on specific criteria (Appendix 2) for the DFA. However, the lower classification success of some topographic maps suggests that some observed retinal specializations may be intermediate between two different types. Our method has the potential to quantify this degree of variability.

One trait that could facilitate the discrimination of an *area* from a visual streak in the future is the spatial extent of these retinal specializations. It is assumed that *areae* are smaller than visual streaks (Collin, 1999; Hughes, 1977). Although the spatial limits of foveae are easier to distinguish morphologically from the whole-mounted retina (e.g., the width of the foveal pit), the same does not apply to *areae* and visual streaks. For instance, the *area* is defined as a thickening of the retinal tissue; however, there is no established criterion to determine where the thickening begins in a cross-section, let alone in a topographic map. The same is true for the visual streak, as the density thresholds that bound the band of high cell density (hence, spatial resolving power) across the retina are yet to be established. Our method actually identified species that can be used to better understand the morphological differences between *areae* and visual streaks by comparing the aforementioned retinal traits in species that were correctly as well as incorrectly classified. Future work addressing the spatial limits of retinal specializations (e.g., expressed as the percentage of the peak RGC density) could improve the classification success of DFAs like the one used in this study.

Our method has some shortcomings. First, measuring the position of the center of the retinal specialization and the ganglion cell density gradient assumes that cell density increases from the periphery towards a single point of peak density in the retina. Consequently, our method is not applicable to the retinal specialization termed radial anisotropy, which is a concentric increase in ganglion cell density towards the periphery of the retina (Dunlop & Beazley, 1981). Determining the center of this retinal specialization is therefore not feasible using our method. Although the radial anisotropy has been reported in species such as the South African clawed frog *Xenopus laevis* (Dunlop & Beazley, 1984), the sawtoothed eel *Serrivomer beani* (Collin & Partridge, 1996), and Bonapart's spiny eel *Notacanthus bonapartei* (Wagner et al., 1998), it is not very common in vertebrates and is primarily reported in studies that have included amacrine cells within the ganglion cell layer, which may account for the higher cell density in the periphery. Second, our method is at the mercy of the publishing authors having oriented the wholemount correctly with regard to the nasal, dorsal, ventral, and temporal poles and the assumption that the shrinkage of the wholemount during processing was relatively similar in different species (Stone, 1981; Ullmann et al., 2012). Third, our method assumes that the cells counted are all RGCs, which in some cases are difficult to distinguish from other cell types (e.g., amacrine cells; Freeman & Tancred, 1978; Hayes & Holden, 1983; Hughes, 1977; Pettigrew, Dreher, Hopkins, McCall, & Brown, 1988).

Despite these limitations, we believe our novel method can be applied to characterize retinal morphology by standardizing the measurement of retinal traits (retinal specialization position, cell gradient, etc.) from published topographic maps in a wide range of vertebrate taxa. However, when working with taxa with a lower degree of variability in the studied retinal traits, the method can be slightly adjusted. For instance, there are some species with foveae (humans and primates) in which the RGC density increases gradually from the retinal periphery to the center of the retina, and then cell density sharply increases towards

Downloaded from jov.arvojournals.org on 07/19/2019

the fovea and eventually decreases to almost zero at the very center of the fovea. For these species, increasing the number of sampling points in the perifoveal and foveal areas may provide a better characterization of the gradients in cell density. In these cases, the nonlinear approach (even including third order polynomials) may fit the data better.

Although we did not test any specific hypothesis, the retinal traits measured can be used in combination with phylogenetic methods (Garland, Bennett, & Rezende, 2005; Harvey & Pagel, 1991; Nunn & Barton, 2001) to answer questions about the association between retinal morphology and behavioral, ecological, and life-history traits (Hall & Ross, 2007; Heesy, Kamilar, & Willms, 2011), which can shed light onto the evolution of the vertebrate visual system. Additionally, our method can be used to establish how different retinal specializations vary in position, ganglion cell density, and cell density gradients in taxa/species with different visual demands and that inhabit a diversity of ecological niches. Finally, the retinal traits measured can be used to distinguish between different types of retinal specializations using published topographic maps. This may be particularly important for rare, threatened, or endangered species, for example, where the availability of additional retinal material to use for further analysis (such as sectioning the retina in order to confirm the presence or absence of a fovea) is limited due to logistic or ethical considerations.

Acknowledgments

Partial funding for this project was provided to EFJ by the National Science Foundation (IOS-0641550/0937187) and Purdue University. The material presented in this study is based upon work supported by the National Science Foundation through the National Evolutionary Synthesis Center (NESCent) under grant number NSF #EF-0905606.

Commercial relationships: none.
Corresponding author: Esteban Fernández-Juricic.
Email: efernan@purdue.edu.
Address: Department of Biological Sciences, Purdue University, West Lafayette, IN, USA.

References

Akaishi, Y., Uchiyama, H., Ito, H., & Shimizu, Y. (1995). A morphological study of the retinal ganglion cells of the Afghan Pika (*Ochotona rufescens*). *Neuroscience Research, 22*, 1–12.

Beazley, L. (1985). Pattern formation in the retinal ganglion cell layer and visual brain centers. *Australian & New Zealand Journal of Ophthalmology, 13*, 93–102.

Beazley, L., & Dunlop, S. (1983). The evolution of an area centralis and visual streak in the marsupial *Setonix brachyurus*. *Journal of Comparative Neurology, 216*, 211–231.

Binggeli, R. L., & Pauli, W. J. (1969). Pigeon retina: Quantitative aspects of optic nerve and ganglion cell layer. *Journal of Comparative Neurology, 137*, 1–18.

Boire, D., Dufour, J. S., Theoret, H., & Ptito, M. (2001). Quantatative analysis of the retinal ganglion cell layer in the ostrich, *Struthio Camelus*. *Brain Behavior & Evolution, 58*, 343–355.

Bozzano, A. (2004). Retinal specialisations in the dogfish *Centroscymnus coelolepis* from the Mediterranean deep sea. *Scientia Marina, 68*(Suppl. 3), 185–195.

Bozzano, A., & Collin, S. P. (2000). Retinal ganglion cell topography in Elasmobranches. *Brain Behavior & Evolution, 55*, 191–208.

Calderone, J. B., Reese, B. E., & Jacobs, G. H. (2003). Topography of photoreceptors and retinal ganglion cells in the spotted hyena (*Crocuta crocuta*). *Brain Behavior & Evolution, 62*, 182–192.

Coimbra, J. P., Marceliano, M. L. V., Andrade-da-Costa, B. L. D., & Yamada, E. S. (2006). The retina of tyrant flycatchers: Topographic organization of neuronal density and size in the ganglion cell layer of the great kiskadee *Pitangus sulphuratus* and the rusty marginated flycatcher *Myiozetetes cayanensis* (Aves: Tyrannidae). *Brain Behavior & Evolution, 68*, 15–25.

Collin, S. P. (1988). The retina of the shovel-nosed ray, *Rhinobatos batillum* (Rhinobatidae): Morphology and quantitative analysis of the ganglion, amacrine, and bipolar cell populations. *Experimental Biology, 47*, 195–207.

Collin, S. P. (1989). Topography and morphology of retinal ganglion cells in the coral trout *Plectropoma leopardus* (Serranidae): A retrograde cobaltous-lysine study. *Journal of Comparative Neurology, 281*, 143–158.

Collin, S. P. (1999). Behavioural ecology and retinal cell topography. In S. Archer, M. B. Djamgoz, E. Loew, J. C. Partridge, & S. Vallerga (Eds.), *Adaptive mechanisms in the ecology of vision* (pp. 509–535). Dordrecht: Kluwer Academic Publishers.

Collin, S. P. (2008). A web-based archive for topographic maps of retinal cell distribution in verte-

Downloaded from jov.arvojournals.org on 07/19/2019

brates. *Clinical & Experimental Optometry, 91*, 85–95.

Collin, S. P., & Ali, M. A. (1994). Multiple areas of acute vision in two freshwater teleosts, the creek chub, *Semotilus atromaculatus* (Mitchill) and the cutlips minnow, *Exoglossum maxillingua* (Lesueur). *Canadian Journal of Zoology, 72*, 721–730.

Collin, S. P., Hoskins, R. V., & Partridge, J. C. (1997). Tubular eyes of deep-sea fishes: A comparative study of retinal topography. *Brain Behavior & Evolution, 50*, 335–357.

Collin, S. P., Lloyd, D. J., & Wagner, H. J. (2000). Foveate vision in deep-sea teleosts: A comparision of primary visual and olfactory inputs. *Philosophical Transactions of the Royal Society of London B, 355*, 1315–1320.

Collin, S. P., & Northcutt, R. G. (1993). The visual system of the Florida garfish, *Lepisosteus platyrhincus* (Ginglymodi). III. Retinal ganglion cells. *Brain Behavior & Evolution, 42*, 295–320.

Collin, S. P., & Partridge, J. C. (1996). Fish vision: Retinal specialization in the eyes of deep-sea teleosts. *Journal of Fish Biology, 49*(Suppl. A), 157–174.

Collin, S. P., & Pettigrew, J. D. (1988a). Retinal topography in reef teleosts: I. Some species with well-developed areae but poorly-developed streaks. *Brain Behavior & Evolution, 31*, 269–282.

Collin, S. P., & Pettigrew, J. D. (1988b). Retinal topography in reef teleosts: II. Some species with prominent horizontal streaks and high-density areae. *Brain Behavior & Evolution*, *31*, 283–295.

Collin, S. P., & Pettigrew, J. D. (1989). Quantitative comparison of the limits in visual spatial resolution set by the ganglion cell layer in twelve species of reef teleosts. *Brain Behavior & Evolution, 34*, 184–192.

Collin, S. P., & Shand, J. (2003). Retinal sampling and the visual field in fishes. In S. P. Collin & N. J. Marshall (Eds.), *Sensory processing in aquatic environment* (pp. 139–169). New York: Springer-Verlag.

Costa, B. L. S. A., Pessoa, V. F., Bousfield, J. D., & Clarke, R. J. (1987). Unusual distribution of ganglion cells in the retina of the three-toed sloth (*Bradypus variegatus*). *Brazilian Journal of Medical & Biology Research, 20*, 741–748.

Cronin, T. W. (2005). The visual ecology of predator-prey interactions. In P. Barbosa & I. Castellanos (Eds.), *Ecology of predator-prey interactions* (pp. 105–138). Oxford: Oxford University Press.

Curcio, C. A., & Allen, K. A. (1990). Topography of ganglion cells in human retina. *Journal of Comparative Neurology, 300*, 5–25.

DeBruyn, E. J., Wise, V. L., & Casagrande, V. A. (1980). The size and topographic arrangement of retinal ganglion cells in the galago. *Vision Research, 20*, 315–327.

Dolan, T., & Fernández-Juricic, E. (2010). Retinal ganglion cell topography of five species of ground foraging birds. *Brain Behavior & Evolution, 75*, 111–121.

Donascimento, J. L. M., Donascimento, R. S. V., Damasceno, B. A., & Silveira, L. C. L. (1991). The neurons of the retinal ganglion-cell layer of the guinea pig: Quantitative analysis of their distribution and size. *Brazilian Journal of Medical & Biological Research, 24*, 199–214.

Douglas, R. H., Collin, S. P., & Corrigan, J. (2002). The eyes of suckermouth armoured catfish (*Loricariidae*, Subfamily Hypostomus): Pupil response, lenticular longitudinal spherical aberration, and retinal topography. *Journal of Experimental Biology, 205*, 3425–3433.

Dral, A. G. D. (1972). Aquatic and aerial vision in bottlenose dolphin. *Netherlands Journal of Sea Research, 5*, 510–513.

Dunlop, S. A., & Beazley, L. D. (1981). Changing retinal ganglion cell distribution in the frog *Heleioporus eyrei*. *Journal of Comparative Neurology, 202*, 221–236.

Dunlop, S. A., & Beazley, L. D. (1984). A morphometric study of the retinal ganglion cell layer and optic nerve from metamorphosis in *Xenopus laevis*. *Vision Research, 24*(5), 417–427.

Dunlop, S. A., Moore, S. R., & Beazley, L. D. (1997). Changing patterns of vasculature in the developing amphibian retina. *Journal of Experimental Biology, 200*, 2479–2492.

Fernández-Juricic, E. (2012). Sensory basis of vigilance behavior in birds: Synthesis and future prospects. *Behavioural Processes, 89*, 143–152.

Fernández-Juricic, E., Gall, M. D., Dolan, T., O'Rourke, C., Thomas, S., & Lynch, J. R. (2011). Visual systems and vigilance behaviour of two ground-foraging avian prey species: White-crowned sparrows and California towhees. *Animal Behaviour, 81*, 705–713.

Fernández-Juricic, E., Moore, B. A., Doppler, M., Freeman, J., Blackwell, B. F., Lima, S. L., et al. (2011). Testing the terrain hypothesis: Canada geese see their world laterally and obliquely. *Brain Behavior & Evolution, 77*, 147–158.

Fischer, Q. S., & Kirby, M. A. (1991). Number and

Downloaded from jov.arvojournals.org on 07/19/2019

distribution of retinal ganglion-cells in anubis baboons (*Papio anubis*). *Brain Behavior & Evolution, 37*, 189–203.

Freeman, B., & Tancred, E. (1978). The number and distribution of ganglion cells in the retina of the brush-tailed possum, *Trichosurus vulpecula*. *Journal of Comparative Neurology, 177*, 557–567.

Garland, T., Jr., Bennett, A. F., Jr., & Rezende, E. L. (2005). Phylogenetic approaches in comparative physiology. *Journal of Experimental Biology, 208*, 3015–3035.

Hall, M. I., & Ross, C. F. (2007). Eye shape and activity pattern in birds. *Journal of Zoology, 271*, 437–444.

Harman, A., Abrahams, B., Moore, S., & Hoskins, R. (2000). Neuronal density in the human retinal ganglion cell layer from 1677 years. *Anatomical Record, 260*, 124–131.

Hart, N. S. (2002). Vision in the peafowl (Aves: *Pavo cristatus*). *Journal of Experimental Biology, 205*, 3925–3935.

Harvey, P. H., & Pagel, M. D. (1991). *The comparative method in evolutionary biology*. Oxford Series in Ecology & Evolution, Oxford University Press.

Hayes, B. P., & Holden, A. L. (1983). The distribution of displaced ganglion cells in the retina of the pigeon. *Experimental Brain Research, 49*, 181–188.

Hayes, B., Martin, G. R., & Brooke, M. D. L. (1991). Novel area serving binocular vision in the retina of procellariiform seabirds. *Brain Behavior & Evolution, 37*, 79–84.

Heesy, C. P., Kamilar, J. M., & Willms, J. (2011). Retinogeniculostriate pathway components only scale with orbit convergence in primates and not other mammals. *Brain Behavior & Evolution, 77*, 105–115.

Huberty, C. J. (1994). *Applied discriminant analysis*. New York: Wiley.

Hueter, R. E. (1991). Adaptations for spatial vision in sharks. *Journal of Experimental Zoology, S5*, 130–141.

Hughes, A. (1975). A quantitative analysis of the cat retinal ganglion cell topography. *Journal of Comparative Neurology, 163*, 107–128.

Hughes, A. (1977). The topography of vision in mammals of contrasting life style: Comparative optics and retinal organization. In F. Crescitelli (Ed.), *The visual system in vertebrates: Handbook of sensory physiology* (Vol. VII/5, pp. 615–756). New York: Springer-Verlag.

Inzunza, O., Bravo, H., & Smith, R. L. (1989). Foveal regions of bird retinas correlate with the aster of the inner nuclear layer. *Anatomical Record, 223*(3), 342–346.

Inzunza, O., Bravo, H., Smith, R. L., & Angel, M. (1991). Topography and morphology of retinal ganglion-cells in Falconiforms: A study on predatory and carrion-eating birds. *Anatomical Record, 229*(2), 271–277.

Jeffery, G. (1985). The relationship between cell density and the nasotemporal division in the rat retina. *Brain Research, 347*, 354–357.

Mass, A. M. (1992). Peak density, size, and regional distribution of ganglion cells in the retina of the fur seal *Callorhinus ursinus*. *Brain Behavior & Evolution, 39*, 69–76.

Mass, A. M., & Supin, A. Y. (2000). Ganglion cells density and retinal resolution in the sea otter, *Enhydra lutris*. *Brain Behavior & Evolution, 55*, 111–119.

Mass, A. M., & Supin, A. Y. (2003). Retinal topography of the harp seal *Pagophilus groenlandicus*. *Brain Behavior & Evolution, 62*, 212–222.

Mass, A. M., & Supin, A. Y. (2007). Adaptive features of aquatic mammals' eye. *Anatomical Record, 290*, 701–715.

Mass, A. M., & Supin, A. Y. (2010). Retinal ganglion cell layer of the Caspian seal *Pusa caspica*: Topography and localization of the high-resolution area. *Brain Behavior & Evolution, 76*, 144–153.

Mastronade, D. N., Thibeault, M. A., & Dubin, M. W. (1984). Non-uniform postnatal-growth of the cat retina. *Journal of Comparative Neurology, 228*, 598–608.

McIlwain, J. T. (1996). *An introduction to the biology of vision*. New York: Cambridge University Press.

Meyer, D. B. C. (1977). The avian eye and its adaptations. In F. Crescitelli (Ed.), *The visual system of vertebrates: Handbook of sensory physiology* (Vol. VII/5, pp. 549–612). New York: Springer-Verlag.

Moore, B. A., Doppler, M., Young, J. E., & Fernández-Juricic, E. (2012). Interspecific differences in the visual system and scanning behavior of three forest passerines that form heterospecific flocks. *In revision*.

Nunn, C. L., & Barton, R. A. (2001). Comparative methods for studying primate adaptation and allometry. *Evolutionary Anthropology, 10*, 81–98.

Ota, D., Francese, M., & Ferrero, E. A. (1999). Vision in the grass goby, *Zosterisessor ophiocephalus* (Teleostei, Gobiidae): A morphological and behav-

Downloaded from jov.arvojournals.org on 07/19/2019

ioural study. *Italian Journal of Zoology, 66*, 125–139.

Peichl, L. (1992). Topography of ganglion cells in the dog and wolf retina. *Journal of Comparative Neurology, 324*, 603–620.

Peichl, L., Berhmann, G., & Kroger, R. H. H. (2001). For whales and seals the ocean is not blue: A visual pigment loss in marine mammals. *European Journal of Neuroscience, 13*, 1520–1528.

Pettigrew, J. D., Dreher, B., Hopkins, C. S., McCall, M. J., & Brown, M. (1988). Peak density and distribution of ganglion cells in the retinae of microchiropteran bats: Implications for visual acuity. *Brain Behavior & Evolution, 32*, 39–56.

Provis, J. M. (1979). The distribution and size of ganglion cells in the retina of the pigmented rabbit: A quanitative analysis. *Journal of Comparative Neurology, 185*, 121–138.

Quinn, G. P., & Keough, M. J. (2002). *Experimental design and data analysis for biologists*. Cambridge, UK: Cambridge University Press.

Rapaport, D. H., Wilson, P. D., & Rowe, M. H. (1981). The distribution of ganglion cells in the retina of the North American opossum (*Didelphis virginiana*). *Journal of Comparative Neurology, 199*, 465–480.

Rasband, W. S. (1997–2012). ImageJ, U.S. National Institutes of Health, Bethesda, Maryland, USA, http://imagej.nih.gov/ij/

Ross, C. F. (2004). The tarsier fovea: Functionless vestige or nocturnal adaptation? In C. F. Ross & R. F. Kay (Eds.), *Anthropoid origins: New visions* (pp. 477–537). New York: Kluwer Academic/Plenum Publishers.

Schmid, K. L., Schmid, L. M., Wildsoet, C. F., & Pettigrew, J. D. (1992). Retinal topography in the koala (*Phascolarctos cinereus*). *Brain Behavior & Evolution*, *39*, 8–16.

Schiviz, A. N., Ruf, T., Kuebber-Heiss, A., Schubert, C., & Ahnelt, P. K. (2008). Retinal cone topography of Artiodactyl mammals: Influence of body height and habitat. *Journal of Comparative Neurology, 507*, 1336–1350.

Shand, J., Chin, S. M., Harman, A. M., Moore, S., & Collin, S. P. (2000). Variability in the location of the retinal ganglion cell area centralis is correlated with ontogenetic changes in feeding behavior in the black bream, *Acanthopagrus butcheri* (Sparidae, Teleostei). *Brain Behavior & Evolution, 55*, 176–190.

Silveira, L. C. L., Picanco-Diniz, C. W., & Oswaldo-Cruz, E. (1989). Distribution and size of ganglion cells in the retina of large amazon rodents. *Visual Neuroscience, 2*, 221–235.

Silveira, L. C. L., Picanco-Diniz, C. W., Sampaio, L. F. S., & Oswaldo-Cruz, E. (1989). Retinal ganglion cell distribution in the cebus monkey: A comparison with the cortical magnification factors. *Vision Research, 29*, 1471–1483.

Silveira, L. C. L., Perry, V. H., & Yamada, E. S. (1993). The retinal ganlgion-cell distribution and the representation of the visual field in area-17 of the owl monkey, *Aotus trivirgatus*. *Visual Neuroscience, 10*(5), 887–897.

StatSoft, Inc. (2012). *Electronic statistics textbook*. Tulsa, OK: StatSoft. Internet site: http://www.statsoft.com/textbook/. Accessed January 15, 2012.

Stone, J. (1981). *The wholemount handbook: A guide to the preparation and analysis of retinal wholemounts*. Sydney, AU: Maitland Publications.

Stone, J., & Halasz, P. (1989). Topography of the retina in the elephant *Loxodonta africana*. *Brain Behavior & Evolution, 34*, 84–95.

Tabachnick, B., & Fidell, L. (1996). *Using multivariate statistics* (3rd Ed.) New York: Harper & Row.

Takei, S., & Somiya, H. (2002). Guanine-type retinal tapetum and ganglion cell topography in the retina of a carangid fish, *Kaiwarinus equula*. *Proceedings of the Royal Society of London B, 269*, 75–82.

Tancred, E. (1981). The distribution and sizes of ganglion cells in the retinas of five Australian marsupials. *Journal of Comparative Neurology, 196*, 585–603.

Temple, S., Hart, N. S., Marshall, N. J., & Collin, S. P. (2010). A spitting image: Specializations in archerfish eyes for vision at the interface between air and water. *Proceedings of the Royal Society of London B, 277*, 2607–2615.

Tetreault, N., Hakeem, A., & Allman, J. M. (2004). The distribution and size of retinal ganglion cells in *Cheirogaleus medius* and *Tarsius syrichta*: Implications for the evolution of sensory systems in primates. In C. Ross & R. Kay (Eds.), *Anthropoid origins: New visions* (pp. 449–461). New York: Springer-Verlag.

Tiao, Y. C., & Blakemore, C. (1976). Regional specialisation in golden hamsters retina. *Journal of Comparative Neurology, 168*, 439–457.

Ullmann, J. F. P., Moore, B. A., Temple, S. E., Fernández-Juricic, E., & Collin, S. P. (2012). The retinal wholemount technique: A window to understanding the brain and behaviour. *Brain Behavior & Evolution, 79*, 26–44.

Vilela, M. C. R., Mendonca, J. E. F., Bittencourt, H.,

Downloaded from jov.arvojournals.org on 07/19/2019

Lapa, R. M., Alessio, M. L. M., Costa, M. S. M. O., et al. (2005). Differential vulnerability of the rat retina, suprachiasmatic nucleus and intergeniculate leaflet to malnutrition induced during brain development. *Brain Research Bulletin, 64*, 395–408.

Vitek, D. J., Schall, J. D., & Leventhal, A. G. (1985). Morphology, central projections, and dendritic field orientation of retinal ganglion cells in the ferret. *Journal of Comparative Neurology, 241*, 1–11.

Wagner, H. J., Frohlich, E., Negishi, K., & Collin, S. P. (1998). The eyes of seep-sea fish. II. Functional morphology of the retina. *Progress in Retinal and Eye Research, 17*, 637–685.

Wakakuwa, K., Washida, A., & Fukuda, Y. (1985). Distribution and soma size of ganglion cells in the retina of the eastern chipmunk (*Tamias sibiricus asiaticus*). *Vision Research, 25*, 877–885.

Walls, G. L. (1937). Significance of the foveal depression. *Archives of Ophthalmology*, *18*, 912–919.

Walls, G. L. (1942). *The vertebrate eye and its adaptive radiation*. Bloomfield Hills, MI: Cranbrook Institute of Science.

Wässle, H., & Boycott, B. B. (1991). Functional architecture of the mammalian retina. *Physiological Reviews, 71*, 447–80.

Wässle, H., Grünert, U., Röhrenbeck, J., & Boycott, B. B. (1989). Cortical magnification factor and the ganglion cell density of the primate retina. *Nature, 341*, 643–646.

Wathey, J. C., & Pettigrew, J. D. (1989). Quantitive analysis of the retinal ganglion cell layer and optic nerve of the barn owl *Tyto alba*. *Brain Behavior & Evolution, 33*, 279–292.

Whiteside, T. C. D. (1967). The head movement of walking birds. *Journal of Physiology, 188*, 31P–32P.

Wilhelm, M., & Straznicky, C. (1992). The topographic organization of the retinal ganglion-cell layer of the lizard *Ctenophores-nuchalis*. *Archives of Histology & Cytology, 55*, 251–259.

Wong, R. O. L. (1989). Morphology and distribution of neurons in the retina of the American garter snake *Thamnophis sirtalis*. *Journal of Comparative Neurology, 283*, 587–601.

Appendix 1

List of retinal topographic maps of vertebrates used in this study. Most of these maps are available from the retinal topographic map database: http://www.retinalmaps.com.au/ (Collin, 2008).

Downloaded from jov.arvojournals.org on 07/19/2019

Downloaded from jov.arvojournals.org on 07/19/2019

Class	Order	Family	Genus	Species	Common name	RS	Habitat	References
M	Lagomorpha	Ochotonidae	*Ochotona*	*rufescens*	Afghan pika	VS	T	Akaishi, Uchiyama, Ito, & Shimizu, 1995
M	Proboscidea	Elephantidae	*Loxodonta*	*africana*	African elephant	VS	T	Stone & Halasz, 1989
R	Squamata	Colubridae	*Thamnophis*	*sirtalis*	American garter snake	VS	T	Wong, 1989
Av	Falconiformes	Accipitridae	*Falco*	*sparverius*	American Kestrel	F/F	T	Inzunza, Bravo, Smith, & Angel, 1991
M	Primates	Cercopithecidae	*Papio*	*anubis*	Anubis baboon	F	T	Fischer & Kirby, 1991
Ac	Anguilliformes	Synaphobranchidae	*Synaphobranchus*	*kaupi*	Arrowtooth eel	Ar	A	Collin & Partridge, 1996
Ac	Batrachoidiformes	Batrachoididae	*Halophryne*	*diemensis*	Australian frogfish	VS	A	Collin & Pettigrew, 1988a
Av	Strigiformes	Tytonidae	*Tyto*	*alba*	Barn owl	VS	T	Wathey & Pettigrew, 1989
M	Carnivora	Canidae	*Canis*	*lupus f. familiaris*	Beagle	VS	T	Peichl, 1992
Ac	Scopeliformes	Scopelarchidae	*Scopelarchus*	*michaelsarsi*	Bigfin pearleye	Ar	A	Collin & Partridge, 1996
Av	Ciconiiformes	Cathartidae	*Coragyps*	*atratus*	Black vulture	F	T	Inzunza et al., 1991
Ac	Perciformes	Pomacanthidae	*Pomocanthus*	*semicirculatus*	Blue angelfish	Ar	A	Collin & Pettigrew, 1989
M	Primates	Galagidae	*Otolemur*	*crassicaudatus*	Brown greater galago	Ar	T	DeBruyn, Wise, & Casagrande, 1980
Av	Passeriformes	Icteridae	*Molothrus*	*ater*	Brown-headed cowbird	F	T	Dolan & Fernández-Juricic, 2010
M	Diprotodontia	Phalangeridae	*Trichosurus*	*vulpecula*	Brush-tailed possum	VS	T	Freeman & Tancred, 1978
Av	Passeriformes	Emberizidae	*Pipilo*	*crissalis*	California towhee	F	T	Fernández-Juricic, Gall, et al., 2011
Av	Anseriformes	Anatidae	*Branta*	*canadensis*	Canada goose	VS	T	Fernández-Juricic, Moore, et al., 2011
M	Caviidae	Hydrochoerinae	*Hydrochoerus*	*hydrochaeris*	Capybara	VS	T	Silveira, Picanco-Diniz, & Oswaldo-Cruz, 1989a
Ac	Perciformes	Carangidae	*Carangoides*	*equula*	Carangid fish	VS	A	Takei & Somiya, 2002
Av	Passeriformes	Paridae	*Poecile*	*carolinensis*	Carolina chickadee	F	T	Moore, Doppler, Young, & Fernández-Juricic, 2012
M	Carnivora	Felidae	*Felis*	*catus*	Cat	VS	T	Hughes, 1975
M	Primates	Cebidae	*Cebus*	*apella*	Cebus monkey	F	T	Silveira, Picanco-Diniz, Sampaio, & Oswaldo-Cruz, 1989
R	Squamata	Agamidae	*Ctenophorus*	*nuchalis*	Central netted dragon	VS	T	Wilhelm & Straznicky, 1992
Av	Falconiformes	Accipitridae	*Buteo*	*fuscenses australis*	Chilean eagle	F/F	T	Inzunza et al., 1991
Av	Falconiformes	Falconidae	*Milvago*	*chimango*	Chimango caracara	F	T	Inzunza et al., 1991
Ac	Tetraodontiformes	Balistidae	*Balistoides*	*conspicillum*	Clown triggerfish	VS	A	Collin & Pettigrew, 1989
M	Rodentia	Dasyproctidae	*Dasyprocta*	*aguti*	Common agouti	VS	T	Silveira, Picanco-Diniz, Oswaldo-Cruz, et al., 1989
Av	Ciconiiformes	Cathartidae	*Gymnogyps*	*californianus*	Condor	F	T	Inzunza et al., 1991
C	Squaliformes	Dalatiidae	*Isistius*	*brasiliensis*	Cookie cutter shark	Ar	A	Bozzano & Collin, 2000
Ac	Perciformes	Serranidae	*Cephalopholis*	*miniatus*	Coral cod	Ar	A	Collin & Pettigrew, 1988a
Ac	Perciformes	Serranidae	*Plectropomus*	*leopardus*	Coral trout	Ar	A	Collin, 1989
Ac	Cypriniformes	Cyprinidae	*Semotilus*	*atromaculatus*	Creek chub	Ar	A	Collin & Ali, 1994

Downloaded from jov.arvojournals.org on 07/19/2019

Class	Order	Family	Genus	Species	Common name	RS	Habitat	References
Ac	Cypriniformes	Cyprinidae	*Exoglossum*	*maxillingua*	Cutlips minnow	Ar	A	Collin & Ali, 1994
C	Squaliformes	Somniosidae	*Centroscymnus*	*coelolepis*	Dogfish	VS	A	Bozzano, 2004
M	Rodentia	Sciuridae	*Tamias*	*sibricus asiaticus*	Eastern chipmunk	VS	T	Wakakuwa, Washida, & Fukuda, 1985
C	Orectolobiformes	Hemiscylliidae	*Hemiscyllium*	*ocellatum*	Epaulette shark	VS	A	Bozzano & Collin, 2000
Av	Passeriformes	Sturnidae	*Sturnus*	*vulgaris*	European starling	F	T	Dolan & Fernández-Juricic, 2010
M	Carnivora	Mustelidae	*Mustela*		Ferret	Ar	T	Vitek, Schall, & Leventhal, 1985
Ac	Lepisosteiformes	Lepisostedae	*Lepisosteus*	*platyrhincus*	Florida garfish	VS	A	Collin & Northcutt, 1993
M	Carnivora	Otariidae	*Callorhinus*	*ursinus*	Fur seal	Ar	A	Mass, 1992
M	Rodentia	Cricetidae	*Mesocricetus*	*auratus*	Golden hamster	Ar	T	Tiao & Blakemore, 1976
Ac	Perciformes	Gobiidae	*Zosterisessor*	*ophiocephalus*	Grass goby	Ar	A	Ota, Francese, & Ferrero, 1999
Av	Passeriformes	Tyrannidae	*Pitangus*	*sulphuratus*	Great kiskadee	F/Ar	T	Coimbra, Marceliano, Andrade-da-Costa, & Yamada, 2006
M	Rodentia	Caviidae	*Cavia*	*porcellus*	Guinea pig	VS	T	Donascimento, Donascimento, Damasceno, & Silveira, 1991
M	Diprotodontia	Vombatidae	*Lasirohinus*	*latiforns*	Hairy-nosed wombat	VS	T	Tancred, 1981
Ac	Perciformes	Labridae	*Choerodon*	*fasciata*	Harlequin tuskfish	VS/Ar	A	Collin & Pettigrew, 1988b1
M	Carnivora	Phocidae	*Pagophilus*	*groenlandicus*	Harp seal	Ar	A	Mass & Supin, 2003
M	Rodentia	Muridae	*Rattus*	*norvegicus*	Hooded rat	Ar	T	Jeffery, 1985
Av	Passeriformes	Fringillidae	*Carpodacus*	*mexicanus*	House finch	F	T	Dolan & Fernández-Juricic, 2010
Av	Passeriformes	Passeridae	*Passer*	*domesticus*	House sparrow	F	T	Dolan & Fernández-Juricic, 2010
M	Diprotodontia	Phascolarctidae	*Phascolarctos*	*cinereus*	Koala	Ar	T	Schmid, Schmid, Wildsoet, & Pettigrew, 1992
Ac	Osmeriformes	Platytroctidae	*Platytroctes*	*apus*	Legless searsid	F	A	Collin & Partridge, 1996
C	Carcharhiniformes	Carcharhinidae	*Negaprion*	*brevirostris*	Lemon shark	VS	A	Hueter, 1991
Ac	Clupeiformes	Alepocephalidae	*Conocara*	*macropterum*	Longfin smoothhead	F	A	Collin, Lloyd, & Wagner, 2000
M	Rodentia	Cuniculidae	*Cuniculus*	*paca*	Lowland paca	VS	T	Silveira, Picanco-Diniz, et al., 1989
Av	Procellariiformes	Procellariidae	*Puffinus*	*puffinus*	Manx shearwater	VS	T	Hayes, Martin, & Brooke, 1991
Av	Columbiformes	Columbidae	*Zenaida*	*macroura*	Mourning dove	F	T	Dolan & Fernández-Juricic, 2010
M	Primates	Cheirogaleidae	*Cheirogaleus*	*medius*	Mouse lemur	Ar	T	Tetreault, Hakeem, & Allman, 2004

Downloaded from jov.arvojournals.org on 07/19/2019

Class	Order	Family	Genus	Species	Common name	RS	Habitat	References
M	Didelphimorphia	Didelphidae	*Didelphis*	*virginiana*	North American opossum	Ar	T	Rapaport, Wilson, & Rowe, 1981
M	Primates	Aotidae	*Aotus*	*Trivirgatus*	Owl monkey	F	T	Silveira, Perry, & Yamada, 1993
Ac	Syngnathiformes	Aulostomidae	*Aulostomus*	*chinensis*	Painted flutemouth	VS	A	Collin & Pettigrew, 1988b
Av	Galliformes	Phasianidae	*Pavo*	*cristatus*	Peafowl	Ar	T	Hart, 2002
M	Lagomorpha	Leporidae	*Oryctolagus*	*cuniculus*	Pigmented rabbit	VS	T	Provis, 1979
M	Diprotodontia	Macropodidae	*Setonix*	*brachyurus*	Quokka	VS	T	Beazley & Dunlop, 1983
Ac	Perciformes	Lethrinidae	*Lethrinus*	*miniatus*	Red-throated emperor	VS	A	Collin & Pettigrew, 1989
Ac	Perciformes	Blenniidae	*Istiblennius*	*edentulus*	Rippled blenny	Ar	A	Collin, 1989
Av	Columbiformes	Columbidae	*Columba*	*livia*	Rock pigeon	F/Ar	T	Binggeli & Pauli, 1969
Av	Passeriformes	Tyrannidae	*Myiozetetes*	*cayanensis*	Rusty-marginated flycatcher	F/Ar	T	Coimbra et al., 2006
Ac	Clupeiformes	Leptochilichthyidae	*Searsia*	*koefoedi*	Searsid	F	A	Collin & Partridge, 1996
C	Rhinobatiformes	Rhinobatidae	*Glaucostegus*	*typus*	Shovel-nosed ray	Ar	A	Collin, 1988
C	Carcharhiniformes	Scyliorhinidae	*Scyliorhinus*	*canicula*	Small spotted dogfish	VS	A	Bozzano & Collin, 2000
Ac	Osmeriformes	Alepocephalidae	*Rouleina*	*attrita*	Softskin smoothhead	F	A	Collin & Partridge, 1996
Ac	Perciformes	Sparidae	*Acanthopagrus*	*butcheri*	Southern black bream	Ar	A	Shand, Chin, Harman, Moore, & Collin, 2000
M	Peramelemorphia	Peramelidae	*Isoodon*	*obesulus*	Southern brown bandicoot	VS	T	Tancred, 1981
Ac	Osmeriformes	Opisthoproctidae	*Opisthoproctus*	*grimaldii*	Spookfish	Ar	A	Collin, Hoskins, & Partridge, 1997
M	Carnivora	Hyaenidae	*Crocuta*	*crocuta*	Spotted hyena	VS	T	Calderone, Reese, & Jacobs, 2003
Ac	Perciformes	Pomacentridae	*Amblyglyphidon*	*curacao*	Staghorn damselfish	Ar	A	Collin & Pettigrew, 1988a
Ac	Siluriformes	Loricariidae	*Pterygoplichthys*	*pardalis*	Suckermouth armored catfish	Ar	A	Douglas, Collin, & Corrigan, 2002
M	Dasyuromorphia	Dasyuridae	*Sacrophilus*	*harissi*	Tasmanian devil	VS	T	Tancred, 1981
M	Diprotodontia	Macropodidae	*Thylogale*	*billiardieri*	Tasmanian wallaby	VS	T	Tancred, 1981
Ac	Stylephoriformes	Stylephoridae	*Stylephorus*	*chordates*	Threadtail	Ar	A	Collin et al., 1997
M	Pilosa	Folivora	*Bradypus*	*variegatus*	3-toed sloth	Ar	T	Costa, Pessoa, Bousfield, & Clarke, 1987
A	Anura	Hylidae	*Litoria*	*moorei*	Tree frog	Ar	A	Dunlop, Moore, & Beazley, 1997
M	Diprotodontia	Macropodidae	*Dendrolagus*	*doriana*	Tree kangaroo	Ar	T	Hughes, 1975
M	Diprotodontia	Macropodidae	*Macropus*	*fuliginosus*	Western gray kangaroo	VS	T	Beazley, 1985
Av	Passeriformes	Sittidae	*Sitta*	*carolinensis*	White-breasted nuthatch	F	T	Moore, Doppler, Young, & Fernández-Juricic, 2012
Av	Passeriformes	Emberizidae	*Zonotrichia*	*leucophrys*	White-crowned sparrow	F	T	Fernández-Juricic, Gall, et al., 2011
M	Carnivora	Canidae	*Canis*	*lupus*	Wolf	VS	T	Peichl, 1992

Appendix 1. Species are classified as terrestrial (T) or aquatic (A). Abbreviations: C, Chondrichthye; Ac, Actinopterygii; A, Amphibia; R, “Reptilia”; Av, Aves; M, Mammalia; RS, retinal specialization; F, fovea; VS, visual streak; Ar, *area*.

Appendix 2: Criteria used to classify retinal specializations from topographic maps

In most of the retinal specializations (across 88 species, Appendix 1) included in this study, the authors' classification coincided with the general criteria to distinguish between retinal specializations. In general, we followed the authors' classification.

Of the three retinal specialization types we focused on in this study, the fovea is the only one that may be seen as a funnel-shaped mark on the wholemounted retina, although its presence should be confirmed through cross-sectional analysis showing tissue invagination. Many studies using topographic maps of the retinal ganglion cell (RGC) layer marked the presence of the fovea following visual inspection. The other retinal specializations studied (*areae* and visual streaks) are more difficult to classify based on the topographic representation of variations in the density of RGCs. Stone and Halasz (1989) emphasized that improving the classification of retinal specializations requires analyses beyond topographic maps; such as establishing the projections of the RGCs to centers in the brain.

Many of the topographic maps published already do not have further tests to confirm the type of retinal specializations. Nevertheless, by following some criteria from the literature (Collin, 2008; Hughes, 1977; Walls, 1937), we classified the three types of retinal specializations based on features detectable by examination of retinal topographic maps. In general terms, we considered the foveas an indentation of the retina showing a funnel-shaped pit in the retinal tissue (Collin, 2008; Walls, 1937). We considered the area as a round, localized concentration of ganglion cells without a noticeable pit in the retinal tissue (Hughes, 1977). Finally, we considered the visual streak as a "bandlike area" crossing along the retina (Hughes, 1977).

However, in some cases, the authors did not specify a type of retinal specialization or their classification did not follow necessarily the criteria presented above. We explain in the following paragraphs the criteria we used to classify these cases.

1. Three-toed sloth (Costa, Pessoa, Bousfield, & Clarke, 1987; http://retinalmaps.com.au//view?tag0=157163). The authors classified this retinal specialization as both an *area* and a visual streak. However, we classified it as an *area* in our analysis. The first two iso-density lines are very circular (greater than 1,350 cells/mm^2), with a concentric increase in RGC density up to a specific point, which follows the area definition (Hughes, 1977). The next two lower cell density isolines (bounding cell densities between 1,000–1,200 cells/mm^2) have a tail that extends in the dorsal direction but not all the way to both sides of the retina. Furthermore, the lines representing even lower cell densities (beyond the fourth highest, less than 1,000 cells/mm^2) do not remain elongated and are more circular.
2. Ferret (Vilela et al., 2005; http://retinalmaps.com.au//view?tag0=157165). The retinal configuration is similar in principle to that of the three-toed sloth, in that the highest cell density ranges (greater than 4,500 cells/mm^2) are circular like an *area*, then the next lower iso-denity line (between 3,500–4,500 cells/mm^2) becomes more elongated in one direction, but the lowest iso-density lines (less than 3,500 cells/mm^2) become more circular. Therefore, we also classified this specialization as an *area*.
3. The topographic maps of seven species of birds (California towhee and white-crowned sparrow, Fernández-Juricic, Gall, et al., 2011; European starling, brown-headed cowbird, house sparrow, house finch, and mourning dove, Dolan & Fernández-Juricic, 2010) were originally reported as having an *area* due to the lack of cross-sections. However, we confirmed through visual examination of their whole-mounted retinas that they have a funnel-shaped pit in the retinal tissue. Therefore, we classified them as all having foveae.
4. The topographic maps from seven species of birds (great kiskadee: http://retinalmaps.com.au//view?tag0=156862; rusty-marginated flycatcher: http://retinalmaps.com.au//view?tag0=156863, Coimbra, Marceliano, Andrade-da-Costa, & Yamada, 2006; Chilean eagle: http://retinalmaps.com.au//view?tag0=156965; American kestrel [sparrow hawk]: http://retinalmaps.com.au//view?tag0=156964; Chimango caracara: http://retinalmaps.com.au//view?tag0=156966; condor: http://retinalmaps.com.au//view?tag0=156967; and black vulture: http://retinalmaps.com.au//view?tag0=156968, Inzunza et al., 1991) all possess both (a) a central fovea, and (b) either a temporal fovea or a temporal *area*. For the maps of the great kiskadee, rusty-marginated flycatcher, Chilean eagle, and American kestrel, we coded both the central specialization (fovea in all cases) and the temporal specialization (fovea in Chilean eagle and American kestrel and *area* in great kiskadee and rusty-marginated flycatcher) as they were classified in the original paper. However, for the black vulture, Chimango caracara, and condor, we only coded the central fovea, but not what the authors classified as a temporal *area*. Following the criteria listed above, what the authors classified as a temporal specialization would only be considered a slight increase in ganglion cell density and not a true *area* as there was not a concentric increase in ganglion cell density.

Downloaded from jov.arvojournals.org on 07/19/2019

Also, each of the seven species (great kiskadee, rusty-marginated flycatcher, Chilean eagle, American kestrel, Chimango caracara, condor, and black vulture) was suggested in the original publications to also have a third retinal specialization: a visual streak. However, we did not assign these species as having a visual streak because the streak-like extension is only an effect of the two other specializations being close to one another rather than a distinctive bandlike area of high RGC density across the retina.

5. In situations in which one specialization was present inside of another specialization, we based our coding on the specialization with the largest area of high resolution in the retina, as this seems to be an important factor affecting how animals gather information behaviorally (e.g., through head movements) within their visual fields. More specifically, when there was an *area* inside of a visual streak (e.g., spotted hyena: http://retinalmaps.com.au//view?tag0=156861, Calderone et al., 2003; cat: http://retinalmaps.com.au//view?tag0=156958, Hughes, 1975; Tasmanian devil: http://retinalmaps.com.au//view?tag0=157080, Tancred, 1981; carangid fish, http://retinalmaps.com.au//view?tag0=157077, Takei & Somiya, 2002; clown triggerfish: http://retinalmaps.com.au//view?tag0=156888, Collin & Pettigrew, 1989; painted flutemouth: http://retinalmaps.com.au//view?tag0=156889, Collin & Pettigrew, 1988; red-throated emperor: http://retinalmaps.com.au//view?tag0=157423, Collin & Pettigrew, 1988; barn owl: http://retinalmaps.com.au//view?tag0=156758, Wathey & Pettigrew, 1989; American garter snake: http://retinalmaps.com.au//view?tag0=157090, Wong, 1989), we counted it as a visual streak.

   Additionally, two of the topographic maps included in the analysis (Carolina chickadee and white-breasted nuthatch) are currently in a manuscript in revision (Moore et al., 2012). These two species have a fovea that could be distinguished from the whole-mount (see above).

Appendix 3: Classification functions from the linear and nonlinear discriminant function analyses (DFAs) of terrestrial and aquatic vertebrates

Shown are the classification functions and their coefficients for each type of retinal specialization. RGC, retinal ganglion cell.

	Fovea	*Area*	Visual streak
Constant	−8.60137	−3.00077	−1.23475
Peak RGC density	0.00034	0.00007	0.00005
Lowest RGC density	0.00105	0.00021	0.00009
Temporal slope	−0.80339	0.33622	0.00107
x-coordinate position	1.63501	−3.31182	−2.00614
y-coordinate position	0.69617	−4.69082	−1.10894

Terrestrial species. *Linear DFA model.* $S_{\text{retinal specialization}} = a + b * \text{peak RGC density} + c * \text{lowest RGC density} + d * \text{temporal slope} + e * x\text{-coordinate position} + f * y\text{-coordinate position}$.

	Fovea	*Area*	Visual streak
Constant	−11.3203	−3.59522	−2.94342
Peak RGC density	0.0005	0.00024	0.00025
Lowest RGC density	0.0007	0.00013	−0.00011
PCA temporal	−1.7354	0.38003	−0.06805
x-coordinate position	1.8869	−1.79340	−0.79163
y-coordinate position	2.7918	−3.41312	0.62487
PCA dorsal	−4.0536	−2.57402	−3.63071

Terrestrial species. *Nonlinear DFA model.* $S_{\text{retinal specialization}} = a + b * \text{peak RGC density} + c * \text{lowest RGC density} + d * \text{PCA factor representing a change in cell density in the temporal region of the retina} + e * x\text{-coordinate position} + f * y\text{-coordinate position} + g * \text{PCA factor representing a change in cell density in the dorsal region of the retina}$.

	Fovea	*Area*	Visual streak
Constant	−2.38964	−2.22052	−6.41977
Peak RGC density	0.00012	−0.00004	0.00043
Lowest RGC density	0.00059	−0.00006	0.00004
Nasal slope	−2.19112	1.83658	−5.72918
Temporal slope	−0.19894	0.20869	−0.25415
Dorsal slope	0.31942	−0.20636	−1.08599
x-coordinate position	−1.25112	1.90093	−4.65734
y-coordinate position	−3.90749	0.77298	−2.29086

Aquatic species. *Linear DFA model.* $S_{\text{retinal specialization}} = a + b * \text{peak RGC density} + c * \text{lowest RGC density} + d * \text{nasal slope} + e * \text{temporal slope} + f * \text{dorsal slope} + g * x\text{-coordinate position} + h * y\text{-coordinate position}$.

	Fovea	*Area*	Visual streak
Constant	−5.53234	−1.98571	−2.83120
x-coordinate position	−3.25709	−0.46134	2.05150
PCA temporal	2.59056	−0.09945	0.38005
Lowest RGC density	−0.00018	0.00043	−0.00021
y-coordinate position	−0.52988	−1.97467	2.32646
PCA dorsal	−2.97284	−0.55221	−2.27568
Peak RGC density	0.00013	0.00005	0.00012

Aquatic species. *Nonlinear DFA model.* $S_{\text{retinal specialization}} = a + b * x\text{-coordinate position} + c * \text{PCA factor representing a change in cell density in the temporal region of the retina} + d * \text{lowest RGC density} + e * y\text{-coordinate position} + f * \text{PCA factor representing a change in cell density in the dorsal region of the retina} + g * \text{peak RGC density}$.

Downloaded from jov.arvojournals.org on 07/19/2019